Interleukin 6 drives durable T cell-mediated immunity to pancreatic cancer

Short title: IL-6 drives durable T cell immunity in PDAC

Paige C. Arneson-Wissink[1], Alexandra Q. Bartlett[2], Heike Mendez[1], Xinxia Zhu[1], Peter R. Levasseur[1], Parham Diba[1, 3], Namratha Turuvekere Vittala Murthy[4], Jessica Dickie[1], Matthew McWhorter[2], Antony Jozic[4], Yulia Eygeris[4], Gaurav Sahay[4, 5], Katelyn T. Byrne[6, 7], Gregory D. Scott[8], Robert Eil[2], Aaron J. Grossberg[1, 6, 7, 9]*

[1] Department of Radiation Medicine, Oregon Health & Science University, Portland, OR, USA

[2] Division of Surgical Oncology, Department of Surgery, Knight Cancer Institute, Oregon Health & Science University, Portland, OR, USA

[3] Medical Scientist Training Program, Oregon Health and Science University, Portland, OR, USA

[4] Department of Pharmaceutical Sciences, College of Pharmacy, Oregon State University, Portland, OR, USA

[5] Department of Biomedical Engineering, Oregon Health & Science University, Portland, OR, USA

[6] Department of Cell, Development, and Cancer Biology, Oregon Health & Science University, Portland, OR, USA

[7] Brenden Colson Center for Pancreatic Care, Oregon Health & Science University, Portland, OR, USA

[8] Department of Pathology, Oregon Health & Science University, Portland, OR, 97239, USA

[9] Cancer Early Detection Advanced Research Center, Oregon Health & Science University,

Portland, OR, USA

***Corresponding Author**: Aaron J. Grossberg, 2730 S Moody Ave, Oregon Health and Science University, Portland, OR, 97201, 503-494-9945, grossber@ohsu.edu

Preprint Server: https://doi.org/10.1101/2024.09.26.615308

Word Count: 3583

Grant Support: This work was supported by the National Cancer Institute (PCAW: K99CA286709; GS: R01CA270783; AJG: K08CA245188, R37CA280692, R01CA264133; RE: K08CA256179), the Brenden Colson Center for Pancreatic Care, the Oregon Pancreas Tissue Registry, the Histopathology Shared Resource for pathology studies (University Shared Resource Program at Oregon Health and Sciences University and the Knight Cancer Institute (P30 CA069533 and P30 CA069533 13S5)), the OHSU Flow Cytometry Shared Resource (OHSU Knight Cancer Institute NCI Cancer Center Support Grant P30CA069533), and the Advanced Multiscale Microscopy Shared Resource (OHSU Knight Cancer Institute, NIH P30 CA069533). RE was also supported by grants from the American Association of Cancer Research, ASCO, and Pancreatic Cancer Action Network.

Data Transparency: All data will be available on the public repository, Mendeley Data, upon publication. Further information and resources, including plasmid sequences, engineered KPC cells, and raw data will be shared upon reasonable request to Aaron J. Grossberg (grossber@ohsu.edu).

41 **Disclosures:** GS is a co-founder of EnterX Bio and has an advisory role to Rare Air Inc.,
42 Serina Tx, and Mana Bio. KTB receives consultation feed from Guidepoint Global and royalties
43 from the University of Pennsylvania for licensed research cell lines. The other authors declare
44 no conflicts. RE is a paid consultant and conducts ongoing research for Lyell Immunopharma.
45 AJG is a paid consultant for Endevica Bio, Inc.

46 **Abbreviations:**

47 BSR	Blasticidin Resistance
48 CAR	Chimeric Antigen Receptor
49 CD	Cell Differentiation
50 ELISA	Enzyme-Linked Immunosorbent Assay
51 Fbxo32	F-Box Protein 32
52 Foxp3	Forkhead Box Protein P3
53 H&E	Hematoxylin and Eosin
54 IL-6	Interleukin 6
55 KPC	$Kras^{G12D/+}$, $Tp53^{R172H/+,}$ Pdx1-Cre
56 NK	Natural Killer
57 OT-PDAC	Orthotopic Pancreatic Ductal Adenocarcinoma
58 PDAC	Pancreatic Ductal Adenocarcinoma
59 Qpcr	Quantitative Polymerase Chain Reaction
60 Trim63	Tripartite Motif Containing 63

61

62 **SYNOPSIS**

63 Interleukin-6 induces rapid and durable T cell-driven immune clearance of pancreatic ductal
64 adenocarcinoma. The anti-tumor immune microenvironment is hallmarked by increased
65 lymphoid aggregate formation, increased CD4 T cell abundance, and decreased Treg
66 abundance.

67 **ABSTRACT**

68 **Background & Aims:** Tumor immune resistance is recognized as a contributor to low
69 survivorship in pancreatic ductal adenocarcinoma (PDAC). The inflammatory cytokine
70 interleukin-6 (IL-6) promotes polarization of CD4 T cell populations away from immune
71 tolerance, and induces differentiation of cytotoxic CD8 T cells. This work aims to test whether
72 IL-6 could stimulate an anti-tumor response in PDAC

73 **Methods:** We overexpressed IL-6 in multiple $Kras^{G12D/+}$, $Tp53^{R172H/+,}$ Pdx1-Cre (KPC) cell lines,
74 which were orthotopically implanted in mice ($OT\text{-}PDAC^{IL6}$). We followed mouse survival and
75 measured tumor growth, tumor histology, and plasma IL-6 at 5 and 10 days after tumor
76 implantation. We measured tumor immune cell infiltration via flow cytometry and histology. We
77 used antibody-based T cell depletion and secondary tumor implantation rechallenge to test the
78 dependency of the durable immune reaction on T cells. We use lipid nanoparticle (LNP)-
79 based delivery of IL-6 mRNA to the pancreas as an orthogonal approach for testing the effect
80 of elevated IL-6 in the tumor microenvironment on anti-tumor T cell invasion.

81 **Results:** Improved survival occurred in all instances of $OT\text{-}PDAC^{IL6}$, with one cell line

(KxPxCx) reproducibly resulting in long-term recurrence-free survival. With KxPxCx cells, circulating IL-6 was 100-fold higher in OT-KxPxCx^{IL6} than in OT-KxPxCx^{parental} mice. Flow cytometry revealed increased T cells and NK cells, and decreased T regulatory cells, and we observed significantly increased lymphoid aggregates in OT-KXPXCX^{IL6} as compared to OT--KxPxCx^{parental} tumors. Antibody-based CD4^{+} and CD8^{+} T cell depletion prevented tumor clearance and completely abolished the survival advantage in OT-KxPxCx^{IL6} mice. The anti-tumor immune response to OT-KxPxCx^{IL6} rendered mice immune to re-challenge with OT-KxPxCx^{parental} tumors. LNP delivery of IL-6 to the pancreas elevated systemic IL-6 levels ~50 fold, lowered tumor burden, and increased anti-tumor T cell phenotypes.

Conclusions: Locally high IL-6 concentrations potently enhance the T cell-mediated anti-tumor response to PDAC.

Key words: Interleukin 6; Pancreatic Ductal Adenocarcinoma; T regulatory cells

95 **INTRODUCTION**

96 Pancreatic ductal adenocarcinoma (PDAC) is associated with an immunosuppressive
97 microenvironment, characterized by low numbers of infiltrating T cells and relatively higher
98 numbers of immunosuppressive T regulatory cells (Tregs)[1, 2]. Despite clinical trials that have
99 established the safety of immunotherapies in PDAC, the immune profile of PDAC limits the
100 clinical efficacy of these interventions[3]. Conversely, increased T cell infiltration with low Treg
101 infiltration is associated with improved patient survival [5]. Strategies that promote T cell
102 activation, such as agonizing CD40 antibodies, increase tertiary immune structure formation
103 and benefit mouse survival in pre-clinical models[4]. A small but growing body of literature
104 suggests that tumor-localized expression of immunomodulatory cytokines, such as IL-6, IL-12,
105 CXCL13, and CCL21 can also improve immune reactivity to tumors by driving localization and
106 differentiation of tumor-infiltrating lymphocytes, which accumulate in tertiary lymphoid
107 structures or lymphoid aggregates[5-7].

108 Interleukin-6 (IL-6) signaling is associated with reduced survival in patients with PDAC
109 attributed to the promotion of tumorigenesis and metastasis [8-11]. Elevated circulating IL-6 also
110 associates with sarcopenia in PDAC patients, and we previously demonstrated that host
111 intrinsic IL-6 signaling is necessary for mice to develop PDAC cachexia[12]. Published literature
112 shows that loss of IL-6 attenuates PDAC development, metastasis, and cachexia onset [12-14].
113 However, IL-6 is also well-established as an immunomodulatory cytokine and contributes to
114 polarization of CD4 T cell populations, differentiation of cytotoxic CD8 T cells, inhibition of
115 inducible Treg development, and expansion and anti-tumor activity in chimeric antigen receptor
116 (CAR) T cell therapies[15-17]. Leveraging the immunomodulatory properties of IL-6 may promote

117 anti-tumor immunity in PDAC.

118 In the current study, we sought to investigate the effect of IL-6 overexpression on immune
119 clearance of PDAC and cachexia development. We used two independent modalities to
120 elevate IL-6 expression in the pancreas: stable IL-6 overexpressing PDAC cells ($PDAC^{IL6}$)
121 from $PDAC^{parental}$ (KPC) cell lines[18], and lipid nanoparticles (LNPs) containing IL-6 mRNA. We
122 found that $PDAC^{IL6}$ cells produced extremely high levels of IL-6 and induced severe cachexia
123 within days of orthotopic implantation (OT-$PDAC^{IL6}$). We also observed dramatic changes in
124 tumor growth dynamics, with one cell line eliciting complete tumor clearance and long-term,
125 recurrence-free mouse survival. IL-6 LNPs targeted the pancreas, caused high levels of
126 circulating IL-6, and limited PDAC tumor growth. We then pursued a series of studies to
127 understand the immune response to high intra-tumoral IL-6. The work shown here presents IL-
128 6 overexpression as a driver of T cell infiltration in PDAC, which poises mice for a favorable
129 anti-tumor immune response.

130 **RESULTS**

131 **Tumor-specific IL-6 overexpression induces spontaneous tumor clearance and**
132 **cachexia recovery.** We developed $PDAC^{IL6}$ cells from the KPC PDAC cell line KxPxCx, using
133 ecotropic retroviral transduction. We first observed that mice implanted with OT-$KxPxCx^{IL6}$
134 tumors experienced nearly 100% survival without reaching terminal endpoints (**Figure 1A**).
135 OT-$KxPxCx^{IL6}$ mice euthanized approximately 10 days after all OT-$KxPxCx^{parental}$ had
136 significantly lower tumor/pancreas mass, and no detectable IL-6 in the plasma (**Figure 1B-C**).
137 Deeper histological assessment of tumors showed that both OT-$KxPxCx^{IL6}$ and OT-

138 KxPxCx^{parental} developed poorly differentiated, infiltrative carcinoma by five days (**Figure 1D-F**).
139 OT-KxPxCx^{IL6} tumors were slightly smaller in mass and histological area than OT-
140 KxPxCx^{parental} tumors (**Figure 1F-G**). By 12 days, OT-KxPxCx^{parental} mice had reached humane
141 euthanasia endpoint, with carcinoma covering approximately 80% of total tissue area, in
142 contrast, OT-KxPxCx^{IL6} tissue was completely devoid of tumor (**Figure 1E,G, Table S1**). We
143 confirmed this result molecularly using qPCR for the codon-optimized *Il6* transgene, which was
144 not detected in OT-KxPxCx^{IL6} whole pancreas tissue after five days (**Figure 1H, Figure S1**).
145 While lung and liver metastases were detected by *Il6* transgene qPCR at five days, there were
146 no metastases detected at 12 days (**Figure S2**). Spontaneous tumor clearance also occurred
147 when KxPxCx^{IL6} cells were implanted subcutaneously, indicating that the phenomenon is not
148 specific to intrapancreatic administration (**Figure S3**).

149 OT-KxPxCx^{parental} plasma IL-6 levels were in line with previously published values, while OT-
150 KxPxCx^{IL6} levels reached 100-fold higher levels at day 5, followed by undetectable levels at
151 later time points (**Figure 1I**) [10, 12]. Because high circulating IL-6 is associated with cachexia
152 development in PDAC, we investigated total body and muscle mass[10]. High plasma IL-6 and
153 peak tumor burden associated with decreased body mass, which recovered with the
154 normalization of IL-6 levels after tumor clearance in the OT-KxPxCx^{IL6} model (**Figure 1J**).
155 Gross muscle mass trended downward at five days and was significantly decreased at 10
156 days, while muscle atrophy gene (*Trim63* and *Fbxo32*) expression was elevated at 5 days and
157 reduced to baseline at 10 days. These data reflect a delay in tissue recovery as the tumor
158 resolves and body mass returns to baseline (**Figure 2K-L**). Collectively, these data show that
159 IL-6 overexpression in PDAC cells leads to severe wasting, followed by body mass recovery
160 upon spontaneous tumor resolution.

161 **Multiple OT-PDAC^{IL6} cell lines, but not CD90.1 transduction control lines, display**
162 **improved survival outcomes.** We then tested whether the impact of IL-6 overexpression on
163 tumor clearance and mouse survival applied to other murine PDAC cell lines: KPC-1199[19],
164 and KPC-1242[20]. While both PDAC^{IL6} cell lines showed significantly improved survival, only
165 OT-1242^{IL6} tumors remained smaller at humane endpoint, when compared to the respective
166 parental control line (**Figure 2A-B, D-E**). High levels of IL-6 overexpression, quantified as
167 plasma IL-6 levels at endpoint, correlated with less tumor burden: 1242^{IL6} caused ~250 fold
168 elevation of IL-6, and 1199^{IL6} did not show a significant overexpression or reduction in tumor
169 mass (**Figure 2C,F**). We validated the clearance and survival phenotypes using an
170 independently generated KxPxCx^{IL6} (KX2^{IL6}) (**Figure 2G-I**). This led us to hypothesize that
171 reduction in tumor mass was driven by IL-6 overexpression. We tested this by using a KxPxCx
172 transduction control cell line, where we expressed CD90.1 alone without IL-6 (OT-
173 KxPxCx$^{CD90.1)}$. OT-KxPxCx$^{CD90.1}$ mice replicated our findings with non-transduced OT-
174 KxPxCx^{parental} mice. Both groups had reached humane euthanasia endpoint by 12 days,
175 carcinoma covering approximately 80% of total tissue area, circulating IL-6 elevated to the
176 expected 200-300 pg/mL range, and body mass loss not exceeding 10% (**Figure 2J-M, Table**
177 **S1**). Finally, we tested the tumor response to IL-6 overexpression when fewer cells are
178 implanted, thus prolonging the period of host exposure to tumor before humane euthanasia
179 criteria are met. We tested 5,000 KxPxCx cells, 100,000 KPC-1199 cells, and 100,00 KPC-
180 1242 cells, and found that survival, tumor mass, and plasma IL-6 replicated our findings with 1
181 million cell implantation doses (**Figure 3A-I**). We therefore concluded that the tumor clearance
182 we observed was specific to IL-6 overexpression and most robust in the KxPxCx cell line,
183 which we selected for continued testing. Because we did not observe a dose-dependent effect,

184 we proceeded to exclusively test the implantation dose of 1 million KxPxCx^{IL6} cells, which
185 aligns with our previously published work.[12]

186 **Tumor IL-6 overexpression induces lymphocytic anti-tumor immune response.** Spleens
187 from OT-KxPxCx^{IL6} mice were significantly enlarged, consistent with IL-6-induced peripheral T
188 cell expansion[15] (**Figure 4A**). We therefore hypothesized that the extreme levels of IL-6
189 generated in the pancreas of OT-KxPxCx^{IL6} mice facilitated immune cell expansion and
190 immune-mediated tumor clearance. We used flow cytometry to evaluate the immune profile of
191 OT-KxPxCx^{IL6} and OT-KxPxCx^{parental} tumors and discovered that pancreata bearing OT-
192 KxPxCx^{IL6} tumors were enriched with CD4^{+} T cells and Natural Killer (NK) cells, while Foxp3^{+}
193 T-regulatory cells were decreased (**Figure 4B-I, S4-5**). We did not identify increases in Th17
194 cells, or Granzyme B^{+} CD8 T cells, which are two phenotypes associated with increased anti-
195 tumor immunity and IL-6 signaling (**Figure S6-7**). We did, however, see a decreased ratio of
196 Foxp3^{+} CD4 T cells to CD8 T cells, indicating a shift towards a less immunosuppressive tumor
197 microenvironment (**Figure 4G**). Because increased tumor-infiltrating lymphocytes are
198 associated with improved outcomes and therapeutic efficacy, we next assessed the
199 localization of T cells relative to tumor cells[21]. By immunofluorescent staining, we found that
200 OT-KxPxCx^{parental} and OT-KxPxCx^{IL6} mice had equal densities of CD3^{+} T cells in both tumor-
201 associated stroma and tumor nests (**Figure 4J-L**). These data initially contradicted the flow
202 cytometry data. However, upon histological assessment, we found that OT-KxPxCx^{IL6}
203 pancreata exhibited a significantly greater number of tumor-associated lymphoid aggregates
204 (**Figure 4M-N**). In PDAC, lymphoid aggregate formation is associated with improved
205 survival[22, 23]. In OT-KxPxCx^{IL6} mice, the lymphoid aggregates were often near, but not
206 necessarily located within the tumor stroma, accounting for the differences between our flow

207 cytometry and immunofluorescence data. In summary, locally high IL-6 induces accumulation
208 of lymphoid aggregates, increased $CD4^+$ T cells, and decreased $Foxp3^+$ T regulatory cells.
209 These conditions favor the hypothesis that tumor clearance occurs via an anti-tumor T cell
210 response.

211 **T cells are necessary for OT-KxPxCx^{IL6} tumor clearance**. We hypothesized that T cells are
212 necessary for OT-KxPxCx^{IL6} tumor clearance, which we tested via antibody-based CD4 and
213 CD8 depletion in tumor-bearing mice, compared to IgG control treatment. Mice received
214 antibody injections two days before tumor implantation and every four days following. We
215 validated T cell depletion via flow cytometry for total T cells (CD90.2), and $CD4^+$ and $CD8^+$
216 cells (**Figure 5A-C**). We followed humane endpoints for the CD4/CD8-depleted group, which
217 reached euthanasia criteria at 8-11 days post-implantation (**Figure 5D**). We euthanized all
218 sham and IgG-treated mice when all CD4/CD8-depleted mice were euthanized, although they
219 were healthy at the time. We used a second engineered cell line, KxPxCx$^{IL6\text{-}LUC}$, which co-
220 expressed IL-6 and luciferase, to measure tumor burden over time. Both OT-KxPxCx$^{IL6\text{-}LUC}$
221 longitudinal data, and OT-KxPxCx^{IL6} endpoint tumor mass data show that CD4/CD8-depletion
222 prevents tumor clearance (**Figure 5E-G**). Histological evaluation by a board-certified
223 pathologist found tumor present in 10/10 CD4/CD8-depleted mice, and in 1/8 IgG control mice
224 (**Figure 5H**). This was supported by *Il6*-transgene qPCR data and plasma IL-6 levels, which
225 showed no elevation of IL-6 in 6/8 IgG-treated PDAC mice (**Figure 5I-J**). We conclude that
226 CD4 and CD8 T cells are necessary for OT-KxPxCx^{IL6} tumor clearance.

227 Because we previously saw recovery of wasting phenotypes in OT-KxPxCx^{IL6} mice as the
228 tumor resolved, we also investigated cachexia resolution in T cell-depleted mice. CD4/CD8

229 depletion prevented body mass recovery and led to sustained muscle wasting as evidenced by
230 decreased muscle mass and increased atrophy-related gene expression (*Trim63, Fbxo32*)
231 (**Figure 5K-M**). The recovery in wasting is therefore directly associated with immune-mediated
232 tumor clearance.

233 **OT-KxPxCx^{IL6} induces a durable T cell response to OT-KxPxCx^{Parental} tumors.** Given the
234 dependency of the anti-OT-KxPxCx^{IL6} response on T cells, which are known to elicit
235 immunologic memory, we hypothesized that OT-KxPxCx^{IL6} tumors would generate a durable
236 immune response that would protect mice in the case of a second tumor exposure. We first
237 tested this hypothesis in a cohort of mice that had recovered from sham surgery or OT-
238 KxPxCx^{IL6} for over two months, and were then rechallenged with OT-KxPxCx$^{parental\text{-}LUC}$
239 (luciferase-expressing) at 76 days after the initial surgery (**Figure 6A**). Sham-recovered mice
240 implanted with KxPxCx$^{parental\text{-}LUC}$ reached euthanasia criteria 13-14 days after rechallenge
241 implantation. In contrast, there were no deaths following rechallenge in the OT-KxPxCx^{IL6}-
242 recovered group (**Figure 6B**). Tumor burden measured longitudinally by IVIS and terminally (in
243 sham-recovered mice only) revealed significant tumor growth only in sham-recovered mice
244 (**Figure 6C-D**). Sham-recovered mice also lost more body mass than OT-KxPxCx^{IL6}-recovered
245 mice following rechallenge (**Figure 6E**). These data indicate that the potent anti-tumor immune
246 response elicited by high concentrations of IL-6 is durable and, once established, not
247 dependent on coincident supraphysiologic IL-6 levels. We then used CD4/CD8 antibody
248 depletion to determine whether the tumor clearance during rechallenge was indeed T cell
249 mediated. In this study, all mice recovered from OT-KxPxCx^{IL6} for 26 days before starting
250 antibody treatment and were given sham surgery or implanted with OT-KxPxCx^{parental} tumors
251 on day 28. We monitored mice for 12 days, until CD4/CD8-depleted mice reached humane

252 euthanasia criteria (**Figure 6F**). We confirmed that clearance of the rechallenge OT-
253 KxPxCx^{parental} tumor is dependent on T cells, which were effectively depleted by the antibody
254 treatment (**Figure 6G-I**). Furthermore, we confirmed that CD4/CD8-depletion does not result in
255 the outgrowth of potentially covert KxPxCx^{IL6} cells, as no tumor was present in any of the OT-
256 KxPxCx^{IL6}-recovered, sham-rechallenged, CD4/CD8-depleted mice (**Figure 6G**). These data
257 show that the T cell response induced by OT-KxPxCx^{IL6} provides durable protection against
258 molecularly similar PDAC tumor growth.

259 **Lipid nanoparticle delivery of IL-6 mRNA replicates the anti-tumor effects observed in**
260 **OT-PDAC^{IL6}.** To test whether the anti-tumor effects of elevated IL-6 in the tumor
261 microenvironment could be derived through a therapeutically-relevant method, we engineered
262 lipid nanoparticles (LNPs) that deliver IL-6 mRNA, are administered by IP injection, and target
263 the pancreas. We used SM-102 LNPs containing luciferase mRNA to validate the particle
264 delivery 6 hours after IP injection in healthy mice (**Figure 7A**). We found that luciferase
265 expression was highest in the pancreas, but was also expressed in the liver, and was nearly
266 undetectable in the spleen (**Figure 7A-B**). Following validation of dosing, we designed an
267 experimental setup with escalating doses of LNPs, which were administered 3 hours prior to
268 OT-PDAC^{parental} (no IL-6 overexpression by the tumor) implantation and every other day after
269 (**Figure 7C**). We included an empty LNP group that was dose-matched for LNP cholesterol
270 content to control for potentially immunogenic effects of the LNPs alone. We found that OT-
271 PDAC^{parental} mice injected with IL-6 LNPs lost significant body mass and had approximately 50-
272 fold higher circulating IL-6 than empty LNP or no LNP control OT-PDAC^{parental} mice (**Figure 7F-**
273 **G**). IL-6 LNP OT-PDAC^{parental} mice euthanized 8 days post-implantation had significantly lower
274 tumor burden and larger spleens (**Figure 7G-H**). We used flow cytometry to evaluate the tumor

275 immune profile and found that tumors from OT-PDAC^{parental} mice injected with IL-6 LNPs did
276 not have significantly more CD4^{+} or CD8^{+} T cells (**Figure 7I-J, S9**). Despite this, there were
277 significantly fewer T-regulatory cells within the CD4 population, and a decreased ratio of
278 Foxp3^{+} CD4 T cells to CD8 T cells in IL-6 LNP-treated OT-PDAC^{parental} mice, replicating our
279 findings in OT-PDAC^{IL6} (**Figure 7K-L**). Finally, we saw significant enrichment of NK and NK T
280 cells in the pancreas of IL-6 LNP-treated OT-PDAC^{parental} mice (**Figure 7M-N**). There were no
281 differences in immune populations between the empty LNP and no LNP groups, suggesting
282 that, in the pancreas with this dosing paradigm, empty SM-102 LNPs did not induce a T cell
283 response. Together, these data show that IL-6 mRNA delivery to the pancreas results in an
284 anti-tumor immune landscape and lower tumor burden in OT-PDAC^{parental} mice.

285 **DISCUSSION**

286 Our model of PDAC IL-6 overexpression induced a robust, rapid, and durable anti-tumor T cell
287 response, accompanied by rapid and severe wasting that recovered as the tumor was cleared.
288 Although IL-6 is traditionally viewed as a negative factor in pancreatic cancer [8-11], we provide
289 evidence that supraphysiologic levels of IL-6, achieved through tumor cell overexpression of
290 IL-6 protein or LNP delivery of IL-6 mRNA, were sufficient to induce an anti-tumor immune
291 landscape in the pancreas. The OT-PDAC^{IL6} tumor microenvironment was characterized by
292 increased lymphoid aggregate formation, elevated CD4^{+} T cells, decreased Foxp3^{+} Treg cells,
293 and elevated NK cells. LNP delivery of IL-6 also drove decreased Treg cell and increased NK
294 cell infiltration. While the KxPxCx tumor line implanted orthotopically exhibited complete,
295 recurrence-free survival, subcutaneous tumors of the same line displayed less complete and
296 slower regression in tumor size. IL-6 overexpression in other KPC cell lines (1199 and 1242)

297 resulted in significant improvements in mouse survival time, although tumors were never fully
298 cleared, and mice progressed to humane euthanasia endpoints. These cases highlighted that
299 the magnitude of anti-tumor immunity due to IL-6 overexpression was partially dependent on
300 cell-line intrinsic properties.

301 Unlike cancer types that are now successfully treated with immunotherapy, survival rates for
302 PDAC patients have increased very slowly over the past decade[24]. PDAC is highly
303 immunosuppressive, causing immunotherapies, such as checkpoint blockade, to be ineffective
304 clinically [25]. Previous work indicated that enhancing T cell activation using exogenous agents,
305 such as agonistic anti-CD40 antibody, improved response to checkpoint blockade therapies
306 and PDAC tumor regression[1]. The Lesinski Group also used IL-6 blockade to enhance the
307 effects of PD-L1 or CTLA4 blockade. Combining checkpoint inhibitors with anti-IL-6 reduced
308 tumor growth and improved T-cell infiltration in implanted murine PDAC models[26, 27]. However,
309 anti-IL-6 was only effective in bolstering the anti-tumor effects of immune checkpoint blockade;
310 the IL-6 antibody did not exert anti-tumor effects on its own. Our work raises a fundamental
311 contradiction regarding the role of IL-6 in PDAC and provides a basis for enhanced IL-6
312 expression as an alternative method to improve T cell response.

313 We propose that the effect of IL-6 on PDAC growth is pleiotropic and concentration-dependent.
314 At low concentrations, IL-6 aids tumor development via signaling directly on neoplastic cells to
315 drive transformation and growth. This is evidenced by the reduced frequency of high-grade
316 pancreatic intraepithelial neoplasia observed in an aggressive genetic model of murine PDAC,
317 when mice were treated with combination PD-L1 and IL-6 blockade[26]. Although some murine
318 PDAC cells produce IL-6, prior work showed that the source of IL-6 in human PDAC tumors

319 and orthotopic mouse models is primarily fibroblasts and immune cells[26, 28]. Combination anti-
320 IL-6 and anti-PD-L1 therapy reduced the number of αSMA+ stromal cells, the loss of which
321 potentially contributed to limiting PDAC progression in that model[26]. Conversely, at
322 supraphysiologic concentrations seen in two independent methods of concentrated IL-6
323 expression in the pancreas (OT-KxPxCx^{IL6} and IL-6 LNP treatment), IL-6 stimulated an anti-
324 tumor immune response. Circulating levels of IL-6 were approximately 100 times higher in OT-
325 KxPxCx^{IL6} and 50 times higher after IL-6 LNP treatment than what we detected in OT-
326 KxPxCx^{parental} mice. We presume that local concentrations in the pancreas were even higher in
327 both systems. We can infer that pancreatic IL-6 is the initiating signal for T cell accumulation
328 and eventual tumor clearance; however, the precise manner in which IL-6 mediates this
329 remains unknown. In addition to increased numbers of tumor-infiltrating T cells, we detected
330 increased NK cells, and decreased Treg cells intratumorally. It is likely that IL-6, which is a
331 known immunomodulatory cytokine, impacted multiple cell populations simultaneously to
332 orchestrate an anti-tumor immune microenvironment[29]. Conversely, it is also likely that lower
333 levels of IL-6 promote expansion of stromal cells, which can contribute to an immune-deplete
334 tumor microenvironment. Future work might investigate how high levels of IL-6, as seen in our
335 OT-KxPxCx^{IL6} model, influence stromal development in PDAC tumors.

336 IL-6 was also established as a driver of acute-phase protein response in the liver, which
337 primed the liver for increased metastasis formation[30]. The KxPxCx cell line used most
338 extensively in this study is not highly metastatic when implanted orthotopically. Liver
339 metastasis was only detected in one mouse at 5 days post-implantation in the OT-KxPxCx^{IL6}.
340 At 12 days post-implantation, zero mice had liver metastases detectable by qPCR (**Figure S2**).
341 Given the high circulating levels of IL-6 in our models, it is likely that STAT3 was activated in

342 hepatocytes, which could contribute to the rapid onset of cachexia in OT-PDAC^{IL6} mice[12].
343 However, we did not directly assess the activation of acute-phase protein response in our
344 model. The rapid resolution of the OT-PDAC^{IL6} primary tumor and micro-metastatic disease
345 made this particular model incompatible with rigorously assessing how supraphysiologic IL-6
346 affected the hepatic metastatic niche. It would be necessary to further investigate the impact
347 of IL-6 on hepatic inflammation if IL-6 elevation were pursued therapeutically in the future, to
348 avoid potentially unexpected negative consequences for metastatic disease.

349 In this work, we confirmed the anti-tumor effects of IL-6 overexpression in PDAC cells using IL-
350 6 LNPs that targeted the pancreas. LNPs are rising in interest as therapeutic vectors for mRNA
351 delivery due to their clinical safety and ability to customize particle content and delivery method
352 to improve tissue-specific targeting[31-34]. Tissue specificity is especially attractive for anti-tumor
353 therapeutic delivery that minimizes off-target effects[35, 36]. Recent publications show that next-
354 generation ionizable lipids can improve pancreas specificity of LNPs[37, 38]. LNP-delivered IL-12
355 was sufficient to prevent PDAC growth[37, 38]. This, and our own work with IL-6, adds to a
356 growing body of literature showing that local expression of immunomodulatory cytokines leads
357 to an anti-tumor T cell response[5-7]. Further work is needed to understand how the T cell
358 response to cytokine overexpression might be conserved and how it could be best translated
359 to clinical use.

360 Our data support the widely-accepted notion that IL-6 induces acutely negative effects, as
361 evidenced by rapid body mass loss of 10-15% in OT-KxPxCx^{IL6} mice and mice that received
362 IL-6 LNPs (**Figure 2H**). In OT-KxPxCx^{IL6} mice, which derived IL-6 expression primarily from
363 the tumor cells, tumor clearance led to rapid recovery in body mass. For patients with PDAC,

364 who are already vulnerable to weight loss, the pro-cachectic effects of IL-6 would likely limit the
365 clinical utility of therapies that elevate IL-6 systemically. Because IL-6 is a secreted protein, it is
366 likely that even pancreas-directed delivery, for example targeted LNP delivery of mRNA, would
367 pose a high risk of side effects for patients. Instead, future work will focus on identifying the
368 immune subpopulations that integrate IL-6 signaling into a T cell response, with the goal of
369 identifying targetable drivers of the anti-tumor response. Using IL-6 overexpression as a model
370 of effective PDAC clearance will open doors to understanding IL-6-mediated T cell activation in
371 PDAC and the intricacies of cachexia resolution after PDAC tumor clearance.

372 **ACKNOWLEDGEMENTS**

373 We thank all members of the Aaron Grossberg, Robert Eil, and Katelyn Byrne, and Gaurav
374 Sahay labs for their helpful discussion and suggestions. We also acknowledge the expert
375 technical assistance by staff in the Advanced Multiscale Microscopy Shared Resource and
376 Histopathology Shared Resource. Author contributions are: Conceptualization, PCAW, AQB,
377 RE, AJG. Methodology, PCAW, AQB, NTVM, AJ, YE, GS, KTB, RE, AJG. Validation, PCAW,
378 AQB, HM, XZ, JD, MM, PRL, PD. Formal Analysis, PCAW, AQB, HM, XZ, JD, PD, GDS, AJG.
379 Investigation, PCAW, AQB, HM, XZ, JD, MM, PRL, PD, GDS. Writing—Original Draft, PCAW.
380 Writing – Review and Editing, PCAW, AQB, KTB, RE, AJG. Visualization, PCAW, AQB, PD.
381 Supervision, RE, AJG. Project Administration, RE, AJG. Funding Acquisition, PCAW, RE, AJG.
382 All authors approved this manuscript.

383 **METHODS**

384 ***Mouse Studies***

385 *Husbandry*

386 C57BL/6J (WT, JAX 000664) mice were purchased from The Jackson Laboratory (Bar Harbor,
387 ME) and maintained in our animal facility. All mice were housed and bred in a dedicated
388 mouse room maintained at 26 °C, 40% humidity, and 12-h light/dark cycle. Mice were provided
389 *ad libitum* access to food and water (5L0D, PicoLab) unless otherwise stated. All mice were 12
390 weeks of age at experiment start. Sex in each experiment is defined in the figure legends.
391 When single housed, mice were allowed a 7-day acclimation period prior to procedure/study
392 start. All tumor studies followed humane endpoints. All mice were humanely euthanized via
393 cardiac puncture or cervical dislocation under deep isoflurane anesthesia. Mouse studies were
394 conducted in accordance with the NIH Guide for the Care and Use of Laboratory animals, and
395 approved by the Oregon Health & Science University IACUC.

396 *Orthotopic Tumor Implantation*

397 A vial of frozen KPC cells was thawed prior to each implantation, and 1 million cells were
398 implanted in 23 uL of PBS per mouse. All mice were anesthetized with isoflurane, scrubbed
399 with betadine, and a para-midline incision was made in the abdomen to expose pancreas. KPC
400 cells or vehicle (PBS) were injected directly into the pancreatic parenchyma. Pancreas was
401 placed back into position and incision was closed using two sutures (4-0 Polysorb) and two
402 skin staples.

403 *Subcutaneous Tumor Implantation*

404 A vial of frozen KPC cells was thawed prior to each implantation, and 1 or 2 million cells were

405 implanted in 100 uL of PBS per mouse. The mouse's lower right abdomen was shaved, then
406 the needle was inserted near the right 4th mammary gland.

407 *Antibody-based depletion*

408 Mice were dosed intraperitoneally (IP) with either a combination of CD4 (BioXcell, #BE0003-1)
409 and CD8a (BioXcell, #BE0061) depletion antibodies, or Rat IgG2b isotype control antibody
410 (BioXcell, #BE0090), which were resuspended in InVivoPure ph7.0 Dilution Buffer (BioXcell,
411 #IP0070) per the manufacturer's instructions. First dose was 0.2 mg each antibody per mouse,
412 given IP two days prior to tumor implantation. Following doses were 0.1 mg each antibody per
413 mouse, given IP every 4 days after initial dose.

414 *Lipid nanoparticle administration*

415 LNPs were injected with a 30g insulin syringe intraperitoneally, following the dosing scheme
416 outlined in Figure 7A and D. LNPs were dosed based off of RNA content and were diluted with
417 calcium- and magnesium-free PBS. Empty LNP dose was calculated by matching the
418 cholesterol content in the empty and IL-6-containing LNPs.

419 *Saphenous blood collection*

420 We collected blood via saphenous bleeds during the LNP study. Mice were restrained by
421 scruffing while occluding the vein, and the hindlimb was wiped with petroleum jelly to expose
422 the vein. A 23G needle was used to gently prick the saphenous vein. Blood was collected in
423 EDTA-treated tubes, which were then placed on ice. Bleeding was stopped with pressure and

424 mice were returned to the cage. Each bleed alternated between left and right hindlimb.
425 Approximately 40 uL of blood was collected at each timepoint. Samples were spun down for 20
426 minutes at 2,000xg and plasma was stored at -80C.

427

428 ***Cell lines***

429 *Growth Conditions and validation*

430 All cells were maintained at 37°C and 5% CO_2 in a humidified incubator, and tested negative in
431 house for mycoplasma using Universal Mycoplasma Detection Kit (30-1012K). *Kras*$^{G12D/+}$,
432 *Tp53*$^{R172H/+}$, *Pdx1-Cre* (KPC) cell lines was generously shared by Dr. Elizabeth Jaffee
433 (KxPxCx) and Dr. David Tuveson (1199 and 1242)[18-20, 39]. KPC cells were grown on tissue
434 culture-treated dishes in growth media consisting of RPMI (Gibco) with 10% FBS (Corning)
435 and 1% penicillin/streptomycin (Gibco).

436 *Engineered KPC*

437 KPC cells expressing the surface marker Thy1.1 (CD90.1) with blasticidin resistance (BSR),
438 IL-6 with puromycin resistance, and luciferase with hygromycin resistance, were generated
439 from our stock of KPC cells (female) described above. IL-6 sequence was codon-optimized for
440 efficient expression (**Figure S9**). Platinum-E ecotropic packaging cells were transfected with
441 plasmid DNA encoding MSGV-Thy1.1, MSGV-IL6-Puro, or MSGV-Luciferase as described
442 previously[40]. Retroviral supernatants were spiked with 2ug/mL polybrene and were mixed 1:1
443 with fresh media before adding to 6-well tissue culture treated plates. Cells were spun at

444 2000g for 90min, 32C, no brake. Cells were then incubated at 37C for 48 hours before
445 washing off the viral supernatant and adding DMEM media (Gibco) supplemented with 10%
446 FBS (Corning). Two days later, KPC cells were placed in complete DMEM media containing
447 puromycin (5ug/mL) and/or blasticidin (5ug/mL) and/or hygromycin (500 ug/mL) to select for
448 transduced cells. Following antibiotic selection, successful transduction was confirmed via flow
449 cytometry staining for Thy1.1. KxPxCx$^{CD90.1}$, KxPxCx^{IL6}, and KxPxCx^{LUC} cells were implanted
450 for OT-PDAC as described for parental KPC cells. Continued culturing of engineered cells was
451 done in selection media described.

452 ***Flow cytometry***

453 *Brefeldin A injections:* For intracellular cytokine staining for flow cytometry, we followed
454 previously published protocols for golgi transport blockade[41]. Briefly, each mouse received
455 100ug Brefeldin A (Selleckchem) injected retro-orbitally 5 hours prior to tissue collection.

456 *Sample preparation*
457 We collected tumors from mice 5 days post implantation, and tumors were weighed, then
458 placed in PBS on ice. Tumor tissue was minced and digested (7). After dissociation, we
459 strained tumor suspension through at 100 um filter, and performed ACK lysis. We collected
460 spleens from mice at the endpoint specified. Spleens were pressed through a 70 um filter,
461 rinsed with PBS, pelleted at 1500 RPM for 5 minutes, and lysed with ACK lysis.

462 *Staining*
463 We stained samples with live/dead stain (1:2000) and surface protein antibodies (1:200 each),
464 and incubated for 20 minutes room temperature (**Table S3**). After staining, we washed

465 samples with FACS buffer and pelleted. For intracellular staining (Foxp3), we fixed and
466 permeabilized cells with 4% paraformaldehyde (BD Cytofix/Cytoperm), washed cells, and then
467 resuspended cells in antibody diluted 1:200 in permeabilization buffer (BD Perm/Wash) with
468 overnight incubation at 4C . The next day we washed and resuspended cells with FACS buffer
469 prior to analysis.

470 *Instrumentation and analysis*

471 All samples were analyzed in the OHSU Flow Cytometry Shared Resource using the Cytek
472 Aurora flow cytometer (Cytek Biosystems), data was analyzed in FlowJoTM v10.8.1. Samples
473 were first gated according to size and single cells, then all live cells were captured. The live
474 population was gated on CD45+ cells to capture all leukocytes. To identify T cells, leukocytes
475 were gated on CD90.2 then sub-gated for CD4+ or CD8+ cells. The CD4+ T cell population
476 was gated on Foxp3 to assess T regulatory cells. Natural killer (NK) cells were sub-gated from
477 the parental CD45+ gate. All NK1.1+ cells were captured, and then divided by expression of
478 CD90.2 to classify as NK (conventional, CD90.2-) or NK T cells (CD90.2+).

479 ***Histology***

480 Pancreas/tumor tissue was fixed overnight in 4% PFA, then stored in 70% ethanol. Tissues
481 were paraffin embedded, sectioned, and hematoxylin and eosin (H&E) stained by the OHSU
482 Histopathology Shared Resource. Tumor tissue was sectioned in 5um slices at levels 50 um
483 apart. H&E stained tumor cross-sections were evaluated by a board-certified gastrointestinal
484 pathologist. All samples were blinded during sectioning/staining and during evaluation. 3-5
485 depths of tissue were qualitatively assessed per mouse. For day 5 tumor samples, 2 depths of

486 tissue were quantified per mouse and averaged together. For day 12 tumor samples, 1 section
487 was quantified.

488 ***Immunofluorescent staining and quantification***

489 Pancreas/tumor tissue was dissected, transferred to BD Cytofix/Cytoperm diluted to 1% PFA,
490 and kept at 4C overnight. Tissue was then transferred to 30% sucrose in PBS and kept at 4C
491 overnight. Tissue was then washed twice in PBS before embedding in OCT media (Sakura).
492 Tissue was cut at 8 um onto superfrost plus slides and stored at -80C until staining. To stain,
493 slides were washed with PBS, blocked with 2.5% BSA 0.3% TritonX in PBS for one hour,
494 stained with pre-conjugated antibodies (**Table S3**) for 1h, washed with PBS, quenched with
495 TrueView Autofluorescence Quench kit (Vector, SP-8400) 2-5 min, stained with DAPI diluted
496 1:1000 for 10 min, and mounted with Vectashield Vibrance mounting medium (Vector, H-
497 1700). Whole tissue sections were imaged on a Zeiss Axio Scan 7 at 20x magnification. Two
498 tissue sections at least 344 um apart were assessed per sample. All images were blinded prior
499 to annotation and analysis. In QuPath (V0.5.1), areas of tumor, as defined as PanCK positive,
500 and stroma, as defined as PanCK negative abnormal tissue, were annotated. Adjacent tissue
501 sections were stained with H&E and used as reference for areas of stroma. Annotations were
502 made using only the DAPI and PanCK stains. After annotation, $CD3^+$ cells ($CD3^+$, $DAPI^+$,
503 PanCK-) were manually counted in stroma and tumor areas. Final counts were normalized to
504 total area of stroma or tumor annotation.

505 ***IVIS imaging***

506 *In vivo*

507 Mice were injected with 100 uL of 15 mg/mL D-luciferin potassium salt in DPBS (no Ca, no Mg)
508 (GoldBio, #LUCK-100), then anesthetized with isoflurane. 10 minutes later, a luminescent
509 image and photo were captured. Longitudinal data was analyzed in one batch by normalizing
510 tumor ROI luminescence total counts to average background ROI luminescence total counts.

511 *Ex vivo*

512 Organs for analysis were placed in PBS on ice immediately following dissection. When all
513 organs were collected, PBS was replaced with 1 mL of 15 mg/mL D-Luciferin in DPBS (no Ca, no
514 Mg) (GoldBio, #LUCK-100). Organs were incubated for 5 minutes before removing from
515 solution, patting dry, and arranging on the IVIS imaging tray. Luminescent image and photo
516 were captured. Total luminescence counts were normalized to background luminescence
517 counts.

518 ***Lipid nanoparticle (LNP) preparation***

519 LNPs were prepared using microfluidic mixing of ethanol (lipid) and aqueous (mRNA) phases
520 at a 3:1 volumetric ratio, with a total flow rate of 12 mL per minute using the Ignite system
521 (Precision Nanosystems, BC, Canada). The lipid phase contained ionizable lipid SM102,
522 cholesterol, DSPC, and DMG-PEG2000 at 50/10/38.5/1.5 molar ratios, respectively, diluted in
523 100% ethanol. mRNA was diluted in sterile 50 mM citrate buffer to achieve an N/P ratio of
524 5.67. For empty LNPs, an equivalent amount of citrate buffer was used. After aqueous and
525 lipid solutions were mixed, the LNPs were dialyzed for 4 hours at room temperature, followed
526 by an overnight dialysis against sterile PBS at 4C in 10 kDa Slide-a-Lyzer G3 cassettes
527 (ThermoFisher, MA, USA). Then, LNPs were concentrated by centrifugation using 100k

528 MWCO Amicon ultracentrifugal filters (Millipore Sigma, Burlington, MA) at 3000g and 4C. LNPs
529 were stored at 4C before administration.

530 ***LNP Characterization***

531 Hydrodynamic size and polydispersity of the LNPs were determined with DLS using Stunner
532 (Unchained Labs, Pleasanton, CA). Encapsulation efficiency and concentration of mRNA were
533 determined using a modified Quant-iT RiboGreen RNA assay (ThermoFisher, MA, USA) and a
534 multimode microplate reader. Cholesterol content was determined with the Invitrogen™
535 Amplex™ Red Cholesterol Assay Kit (ThermoFisher, MA, USA).

536 ***Plasma analytes***

537 Plasma was collected, snap frozen in liquid nitrogen, and stored at -80ºC. Plasma
538 concentrations of IL-6 (Biolegend) were measured using ELISA, and read on a plate reader
539 (BioTek).

540 ***Quantitative real-time polymerase chain reaction (qPCR)***

541 We isolated RNA from cell pellets or tissue samples using the E.Z.N.A. Total RNA Kit I
542 (Omega BioTek) and we prepared cDNA using high-capacity cDNA reverse transcription kit
543 (Applied Biosystems). qPCR was run on the ABI 7300 (Applied Biosystems), using TaqMan
544 Fast Advanced PCR master mix (Applied Biosystems) or SYBR Green master mix (Applied
545 Biosystems). Relative expression was calculated using the $\Delta\Delta C_t$ method. To confirm the
546 presence/absence of *Il6 transgene* in tumor-implanted mice, we performed 30 cycles of qPCR

547 on the ABI7300, followed by running the PCR product on a 3% ethidium bromide gel to
548 determine the presence of a band at the expected size of 131 bp. Primers/probes are listed in
549 **Table S2**.

550 ***Statistical Analysis***

551 Specific statistical tests and sample size for each study is indicated in the figure legends. Error
552 bars in figures show SEM. Statistical analyses were performed using GraphPad Prism (version
553 9; GraphPad Software Inc) or JMP Pro (version 16; SAS Institute Inc), and graphs were built
554 using GraphPad Prism (GraphPad Software Inc) statistical analysis software. P values are 2
555 sided with values less than 0.05 regarded as statistically significant.

556 ***Data Availability***

557 All authors had access to the study data and had reviewed and approved the final manuscript.
558 All data will be available on the public repository, Mendeley Data, upon publication. Further
559 information and resources, including plasmid sequences, engineered KPC cells, and raw data
560 will be shared upon reasonable request to Aaron J. Grossberg (grossber@ohsu.edu).

561

562 **FIGURES AND FIGURE LEGENDS**

Figure 1

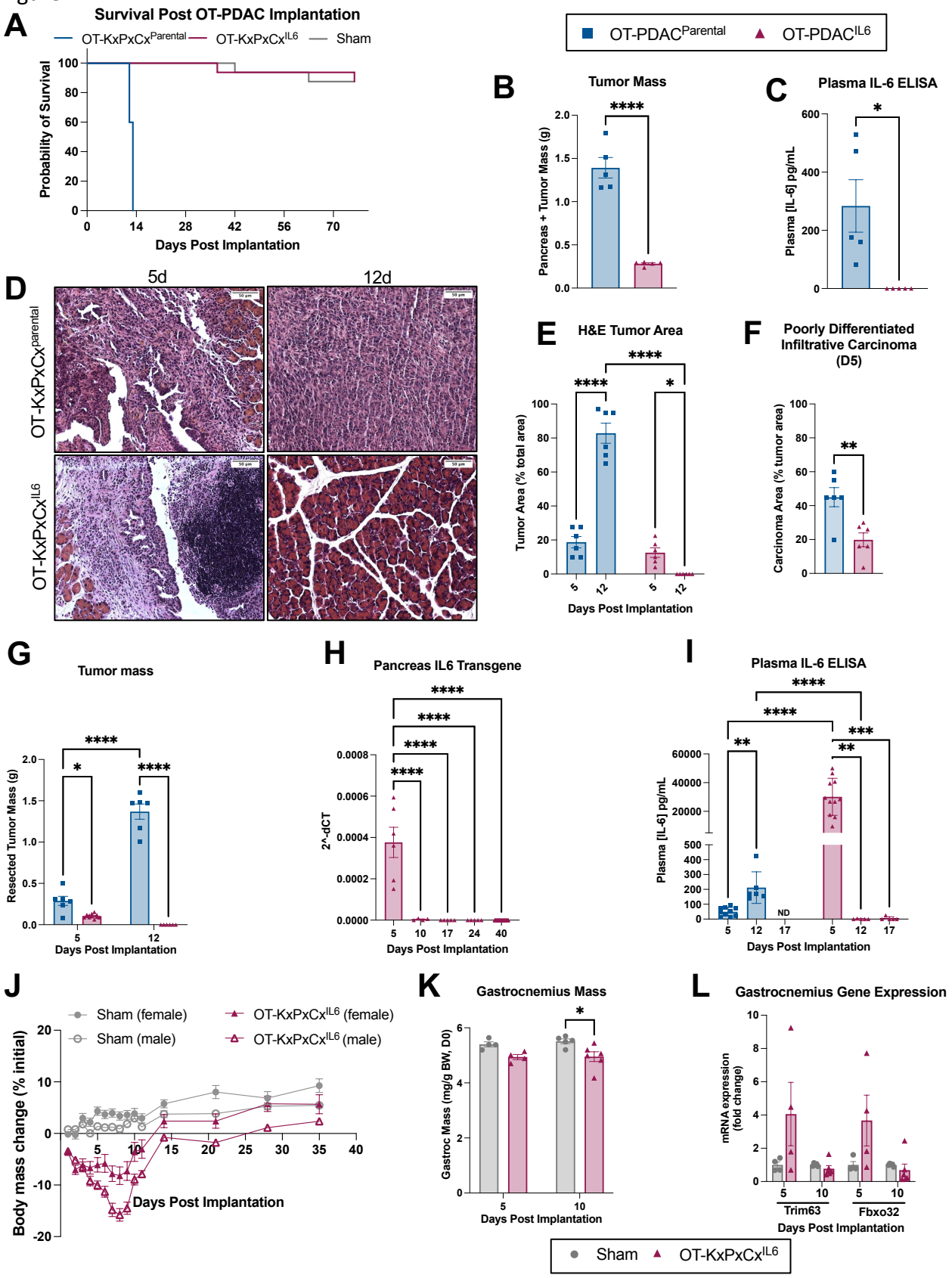
A
Survival Post OT-PDAC Implantation
OT-KxPxCx^Parental
OT-KxPxCx^IL6
Sham
Probability of Survival
Days Post Implantation
OT-PDAC^Parental
OT-PDAC^IL6
B
Tumor Mass
Pancreas + Tumor Mass (g)
C
Plasma IL-6 ELISA
Plasma [IL-6] pg/mL
D
5d
12d
OT-KxPxCx^parental
OT-KxPxCx^IL6
E
H&E Tumor Area
Tumor Area (% total area)
Days Post Implantation
F
Poorly Differentiated Infiltrative Carcinoma (D5)
Carcinoma Area (% tumor area)
G
Tumor mass
Resected Tumor Mass (g)
Days Post Implantation
H
Pancreas IL6 Transgene
2^-dCT
Days Post Implantation
I
Plasma IL-6 ELISA
Plasma [IL-6] pg/mL
ND
Days Post Implantation
J
Sham (female)
Sham (male)
OT-KxPxCx^IL6 (female)
OT-KxPxCx^IL6 (male)
Body mass change (% initial)
Days Post Implantation
K
Gastrocnemius Mass
Gastroc Mass (mg/g BW, D0)
Days Post Implantation
L
Gastrocnemius Gene Expression
mRNA expression (fold change)
Trim63
Fbxo32
Days Post Implantation
Sham
OT-KxPxCx^IL6

563

564 **Figure 1: OT-KxPxCx^{IL6} results in complete tumor clearance and body mass recovery.**
565 (A) Survival comparison of OT-KxPxCx^{Parental} and OT-KxPxCx^{IL6}. N = 8 female, 8 male Sham
566 and OT-KxPxCx^{IL6}, 1 female, 4 male OT-KxPxCx^{parental} mice. Statistically tested with Log-rank
567 (Mantel-Cox) test. (B) Tumor mass at humane endpoint (OT-KxPxCx^{Parental}). Pancreas mass of
568 OT-KxPxCx^{IL6} euthanized at a pre-determined endpoint of 24 days (did not meet humane
569 euthanasia criteria); tumor tissue was not present. Statistically tested with 2-way ANOVA main
570 effects only with Tukey correction for multiple comparisons. (C) Plasma IL-6 levels at the
571 endpoints indicated in (H), Il-6 was below the assay detection limit for OT-KxPxCx^{IL6} mice.
572 Statistically tested with 2-way ANOVA main effects only with Tukey correction for multiple
573 comparisons. (A-C) N = 2 female, 3 male KxPxCx^{IL6}, 1 female, 4 male KxPxCx^{parental} mice. (D)
574 Representative pancreas cross sections at 5 (left) and 10 days (right) from OT-KxPxCx^{parental}
575 (top) and OT-KxPxCx^{IL6} (bottom) tumor implantation. Scale bars represent 50 um (top) and
576 100 um (bottom). (E) Tumor area as a percent of total tissue area at 5 and 12 days, quantified
577 by board-certified pathologist. (F) Percentage of tumor area classified as poorly-differentiated,
578 infiltrative carcinoma at 5 days by board-certified pathologist. (G) Tumor mass at 5 and 12
579 days. (B-D) N = 3 male, 3 female mice per group. (H) Expression of *Il6 transgene* expression,
580 measured by qPCR at 5 (N = 3 male, 3 female), 10 (N = 6 male), 17 (N = 3 male, 2 female), 24
581 (N = 3 male, 2 female), and 40 (N = 16 male, 16 female) days. Statistically tested with One-
582 way ANOVA with Tukey correction for multiple comparisons. (I) Plasma IL-6 measured by
583 ELISA at 5 (N = 10 male KxPxCx^{Parental}, 11 male KxPxCx^{IL6}), 12(N = 3 male, 3 female
584 KxPxCx^{Parental}, 3 male, 2 female KxPxCx^{IL6}), and 17 (N = 2 male, 3 female KxPxCx^{IL6}) days.
585 Statistically tested with 2-way ANOVA main effects only with Tukey correction for multiple
586 comparisons. (J) Body mass change as a percentage of initial body mass over time. N = 8

587 male, 8 female mice per group. Statistically tested with 3-way ANOVA. P<0.0001 for Time,
588 Sex, Tumor Status, Time x Sex, Time x Tumor Status. p=0.0002 for Sex x Tumor Status. p=
589 0.2900 for Time x Sex x Tumor Status. (K) Gastrocnemius muscle mass normalized to initial
590 body mass. (L) Atrophy-related gene expression (*Trim63* and *Fbxo32*) in gastrocnemius
591 muscle, measured by qPCR. (J-L) 5d N = 1 female, 3 male mice per group. 10d N = 6 male
592 PDAC, 5 male sham mice. Error bars represent SEM. Unless otherwise noted, 2x2 studies
593 were statistically tested with a full effects model 2-way ANOVA and Sidak multiple
594 comparisons test. 2-group analysis tested with unpaired t-test. **** P<0.0001, ***P<0.001,
595 **P<0.01, *P<0.05.

596

Figure 2

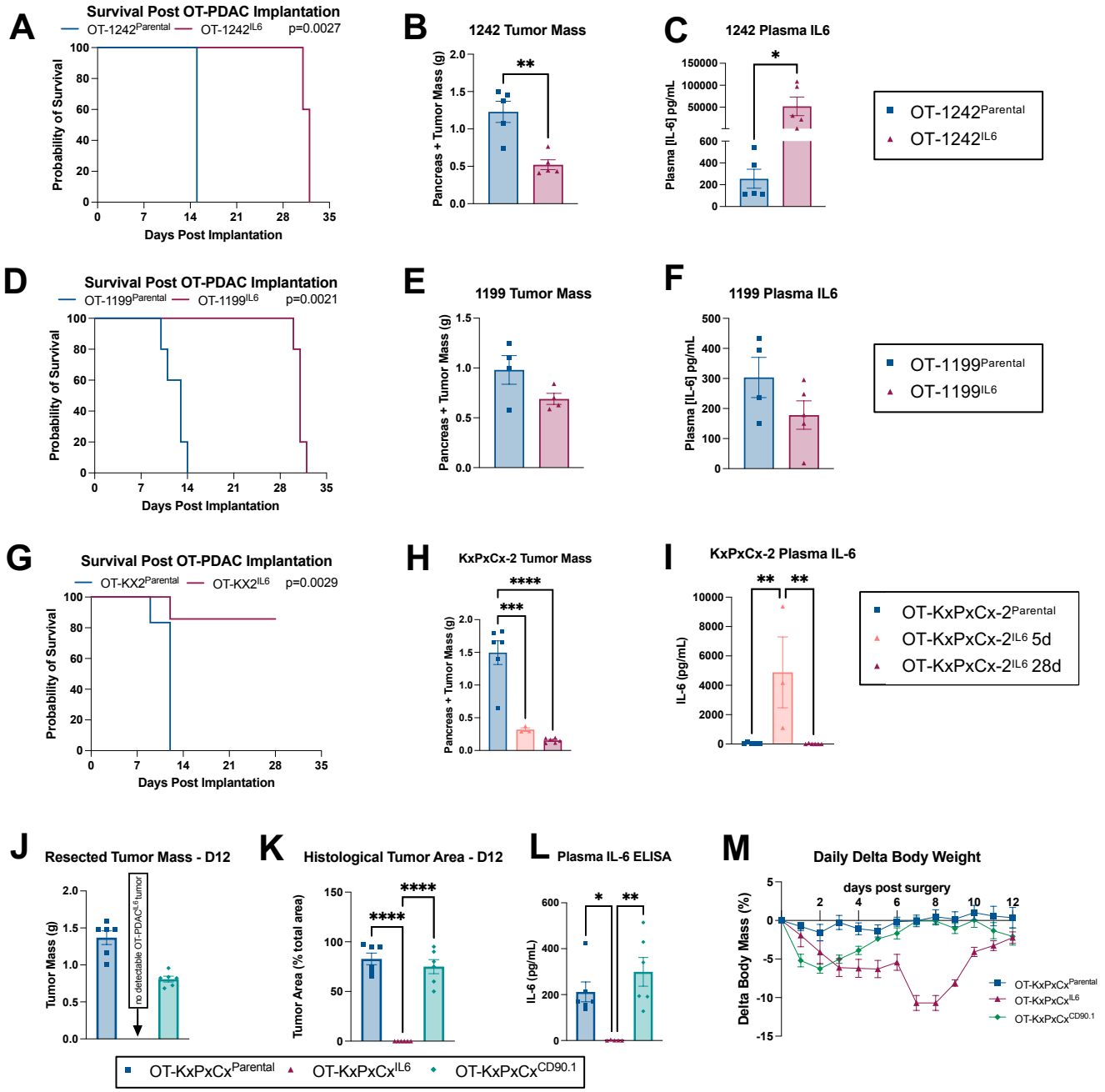
A
Survival Post OT-PDAC Implantation
OT-1242Parental
OT-1242IL6
p=0.0027
Probability of Survival
Days Post Implantation
B
1242 Tumor Mass
Pancreas + Tumor Mass (g)
C
1242 Plasma IL6
Plasma [IL-6] pg/mL
OT-1242Parental
OT-1242IL6
D
Survival Post OT-PDAC Implantation
OT-1199Parental
OT-1199IL6
p=0.0021
Probability of Survival
Days Post Implantation
E
1199 Tumor Mass
Pancreas + Tumor Mass (g)
F
1199 Plasma IL6
Plasma [IL-6] pg/mL
OT-1199Parental
OT-1199IL6
G
Survival Post OT-PDAC Implantation
OT-KX2Parental
OT-KX2IL6
p=0.0029
Probability of Survival
Days Post Implantation
H
KxPxCx-2 Tumor Mass
Pancreas + Tumor Mass (g)
I
KxPxCx-2 Plasma IL-6
IL-6 (pg/mL)
OT-KxPxCx-2Parental
OT-KxPxCx-2IL6 5d
OT-KxPxCx-2IL6 28d
J
Resected Tumor Mass - D12
Tumor Mass (g)
no detectable OT-PDACIL6 tumor
K
Histological Tumor Area - D12
Tumor Area (% total area)
L
Plasma IL-6 ELISA
IL-6 (pg/mL)
M
Daily Delta Body Weight
days post surgery
Delta Body Mass (%)
OT-KxPxCxParental
OT-KxPxCxIL6
OT-KxPxCxCD90.1

598 **Figure 2: Tumor-cell IL-6 overexpression transduction controls.** A) Survival comparison of
599 Sham, OT-1242^{Parental} and OT-1242^{IL6}. Statistically tested with Log-rank (Mantel-Cox) test on
600 pairwise comparisons. (B) Pancreas and tumor mass at humane endpoint. (C) Plasma IL-6
601 levels at humane endpoint. (D) Survival comparison of Sham, OT-1199 ^{Parental} and OT-1199^{IL6}.
602 Statistically tested with Log-rank (Mantel-Cox) test on pairwise comparisons. (E) Pancreas and
603 tumor mass at humane endpoint. (F) Plasma IL-6 levels at humane endpoint. (A-F) N= 5 male
604 mice per group. (G) Survival comparison of Sham, OT-KX2^{Parental} and OT-KX2^{IL6}. Statistically
605 tested with Log-rank (Mantel-Cox) test on pairwise comparisons. (H) Pancreas and tumor
606 mass at humane endpoint (OT-KX2^{Parental}); 5 and 28 days (OT-KX2^{IL6}). Statistically tested with
607 one-way ANOVA. (I) Plasma IL-6 levels at humane endpoint. (G-I) N = 3 male mice OT-KX2^{IL6}
608 d5, 6 male mice OT-KX2^{IL6} d28 and OT-KX2^{parental}. (J-M) Control-transduced PDAC cells (OT-
609 KxPxCx$^{CD90.1}$) do not spontaneously clear. (J) Tumor mass at 12 days post implantation. (K)
610 Tumor area as a percent of total tissue area at 12 days post implantation, quantified by board-
611 certified pathologist. (L) Plasma IL-6 measured by ELISA at 12 days post implantation. (M)
612 Body mass change as a percentage of initial body mass over time. Statistically tested with
613 one-way ANOVA analysis with repeated measures. P<0.0001 for Time and Time x Tumor
614 Status. p=0.0002 for Tumor Status. (J-M) N = 3 male, 3 female mice per group. Error bars
615 represent SEM. Unless otherwise noted, 2-group studies were statistically tested with unpaired
616 t-test. 3-group studies were statistically tested with 1-way ANOVA and Sidak multiple
617 comparisons test. **** P<0.0001, ***P<0.001, **P<0.01, *P<0.05.

618

619

620

Figure 3

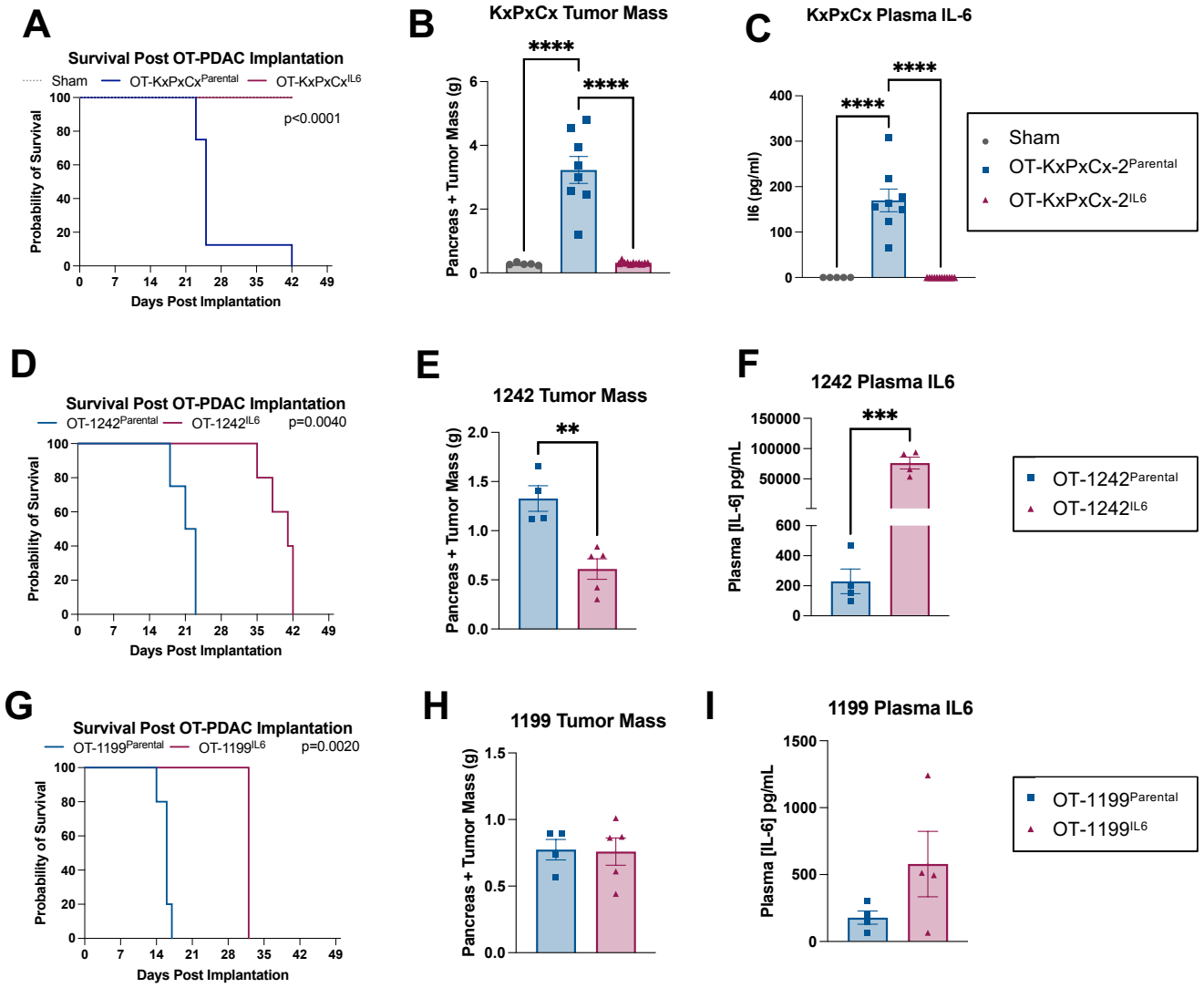
A
Survival Post OT-PDAC Implantation
Sham
OT-KxPxCx Parental
OT-KxPxCx IL6
p<0.0001
Probability of Survival
Days Post Implantation
B
KxPxCx Tumor Mass
****
****
Pancreas + Tumor Mass (g)
C
KxPxCx Plasma IL-6
****
****
Il6 (pg/ml)
Sham
OT-KxPxCx-2 Parental
OT-KxPxCx-2 IL6
D
Survival Post OT-PDAC Implantation
OT-1242 Parental
OT-1242 IL6
p=0.0040
Probability of Survival
Days Post Implantation
E
1242 Tumor Mass
**
Pancreas + Tumor Mass (g)
F
1242 Plasma IL6
***
Plasma [IL-6] pg/mL
OT-1242 Parental
OT-1242 IL6
G
Survival Post OT-PDAC Implantation
OT-1199 Parental
OT-1199 IL6
p=0.0020
Probability of Survival
Days Post Implantation
H
1199 Tumor Mass
Pancreas + Tumor Mass (g)
I
1199 Plasma IL6
Plasma [IL-6] pg/mL
OT-1199 Parental
OT-1199 IL6

621

622 **Figure 3: Effects of tumor-specific IL-6 overexpression are maintained with lower tumor**
623 **inoculation.** (A) Survival comparison of OT-KxPxCx^{Parental} and OT-KxPxCx^{IL6} mice implanted
624 with 5,000 cells. Statistically tested with Log-rank (Mantel-Cox) test on pairwise comparisons.
625 (B) Pancreas and tumor mass at humane endpoint (OT-KxPxCx^{Parental}); 42 days (OT-
626 KxPxCx^{IL6}). (C) Plasma IL-6 levels at endpoint. (A-C) N = 11 male mice (OT-KxPxCx^{IL6}), 8
627 male mice (OT-KxPxCx^{Parental}), and 5 male mice (sham). (D) Survival comparison of Sham,
628 OT-1242^{Parental} and OT-1242^{IL6}. Statistically tested with Log-rank (Mantel-Cox) test on pairwise
629 comparisons. (E) Pancreas and tumor mass at humane endpoint. (F) Plasma IL-6 levels at
630 humane endpoint. (G) Survival comparison of Sham, OT-1199 ^{Parental} and OT-1199^{IL6}.
631 Statistically tested with Log-rank (Mantel-Cox) test on pairwise comparisons. (H) Pancreas and
632 tumor mass at humane endpoint. (I) Plasma IL-6 levels at humane endpoint. Error bars
633 represent SEM. Unless otherwise noted, 2-group studies were statistically tested with unpaired
634 t-test. 3-group studies were statistically tested with 1-way ANOVA and Sidak multiple
635 comparisons test. **** $P<0.0001$, ***$P<0.001$, **$P<0.01$, *$P<0.05$.

636

637

Figure 4

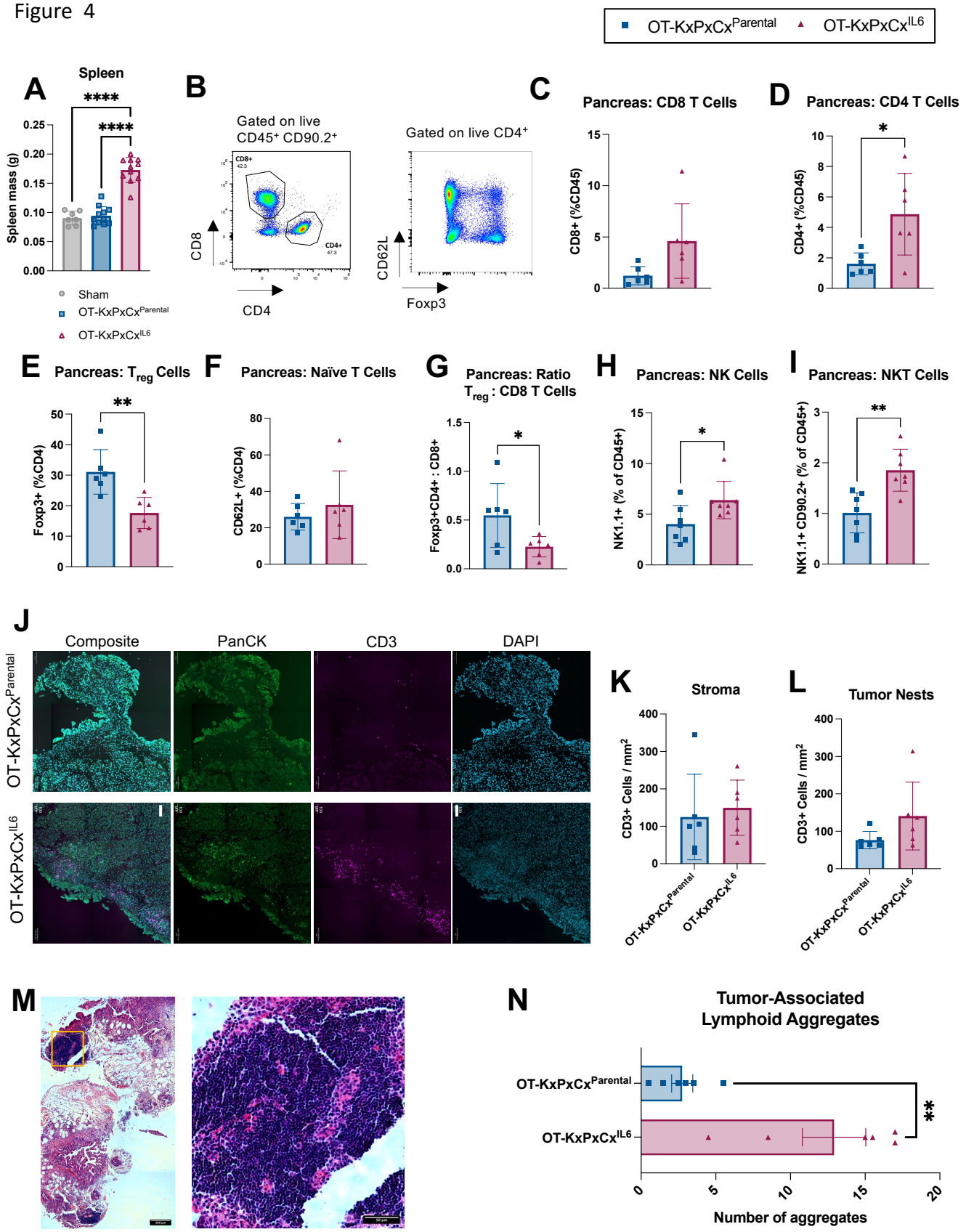
OT-KxPxCx^Parental
OT-KxPxCx^IL6
A
Spleen
Spleen mass (g)
Sham
OT-KxPxCx^Parental
OT-KxPxCx^IL6
B
Gated on live CD45+ CD90.2+
CD8
CD4
Gated on live CD4+
CD62L
Foxp3
C
Pancreas: CD8 T Cells
CD8+ (%CD45)
D
Pancreas: CD4 T Cells
CD4+ (%CD45)
E
Pancreas: Treg Cells
Foxp3+ (%CD4)
F
Pancreas: Naïve T Cells
CD62L+ (%CD4)
G
Pancreas: Ratio Treg : CD8 T Cells
Foxp3+CD4+ : CD8+
H
Pancreas: NK Cells
NK1.1+ (% of CD45+)
I
Pancreas: NKT Cells
NK1.1+ CD90.2+ (% of CD45+)
J
Composite
PanCK
CD3
DAPI
OT-KxPxCx^Parental
OT-KxPxCx^IL6
K
Stroma
CD3+ Cells / mm2
L
Tumor Nests
CD3+ Cells / mm2
M
N
Tumor-Associated Lymphoid Aggregates
OT-KxPxCx^Parental
OT-KxPxCx^IL6
Number of aggregates

638

Figure 4: OT-KxPxCx^{IL6} induces lymphocytic anti-tumor immune response. (A) Spleen mass at 5 days. N = 6 male mice per group. (B-I) Intra-tumoral immune cell populations from pancreas at 5 days: (B) Representative flow gating strategy for T cells. (C) CD8$^+$ T cells, (D) CD4$^+$ T cells, (E) Foxp3$^+$ T regulatory cells, (F) CD62L$^+$ Naive T cells. (G) Ratio of Foxp3$^+$CD4$^+$ to CD8$^+$ cells, representative of a the degree of anti-tumor activity in the tumor microenvironment. (H) NK1.1$^+$ Natural Killer cells, (I) NK1.1$^+$/CD90.2$^+$ NK T cells. (B-F) N = 6 male mice per group. (G-I) N = 4 female, 3 male mice per group. (J) representative images of CD3$^+$ T cell infiltration in tumor and associated stroma of OT-KxPxCx^{parental} (top) and OT-KxPxCx^{IL6} (bottom) mice. Tissues were stained with DAPI (blue), CD3 (magenta), and Pancytokeratin (PanCK, green). (scale bars = 100 um). (K-L) CD3$^+$ cells counted per mm^2 of stroma (K) or tumor nests (L) in immunofluorescence stained pancreas tissues. N = 3 male, 3 female mice per group. (M) Representative H&E image of lymphoid aggregates adjacent to tumor and stroma in OT-KxPxCx^{IL6} pancreas (left) and magnified image of lymphoid aggregate (right). Area of magnification is denoted on left image with orange box. (N) Pathologist-evaluated number of tumor-associated lymphoid aggregates in H&E stained pancreas cross sections from tissue collected at 5 days. N = 3 male, 3 female mice per group. Error bars represent SEM. 2-group analysis tested with unpaired t-test. **** P<0.0001, ***P<0.001, **P<0.01, *P<0.05.

Figure 5

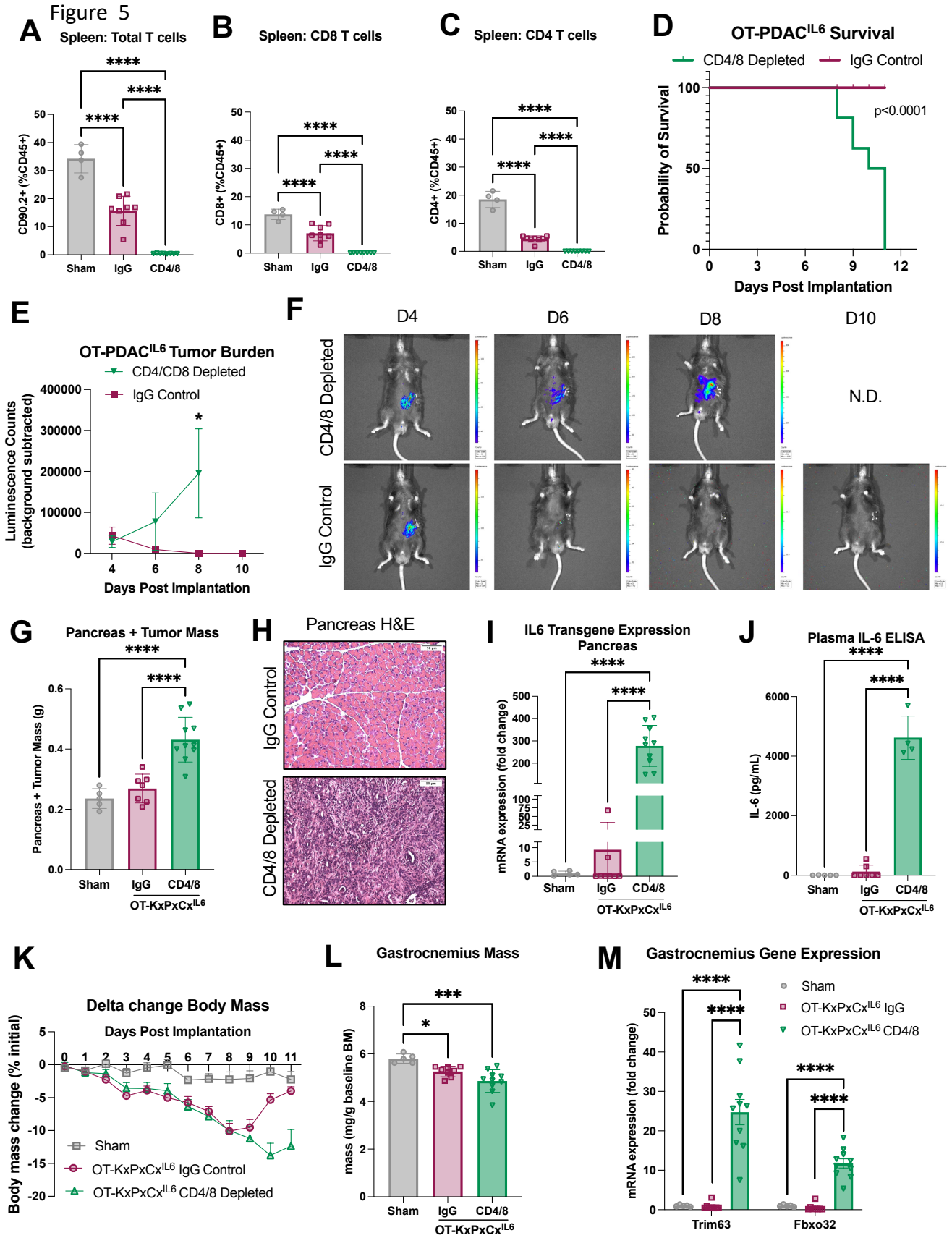
A
Spleen: Total T cells
CD90.2+ (%CD45+)
Sham
IgG
CD4/8
B
Spleen: CD8 T cells
CD8+ (%CD45+)
C
Spleen: CD4 T cells
CD4+ (%CD45+)
D
OT-PDAC^IL6 Survival
CD4/8 Depleted
IgG Control
Probability of Survival
p<0.0001
Days Post Implantation
E
OT-PDAC^IL6 Tumor Burden
CD4/CD8 Depleted
IgG Control
Luminescence Counts (background subtracted)
Days Post Implantation
F
D4
D6
D8
D10
CD4/8 Depleted
IgG Control
N.D.
G
Pancreas + Tumor Mass
Pancreas + Tumor Mass (g)
OT-KxPxCx^IL6
H
Pancreas H&E
IgG Control
CD4/8 Depleted
I
IL6 Transgene Expression Pancreas
mRNA expression (fold change)
OT-KxPxCx^IL6
J
Plasma IL-6 ELISA
IL-6 (pg/mL)
OT-KxPxCx^IL6
K
Delta change Body Mass
Days Post Implantation
Body mass change (% initial)
Sham
OT-KxPxCx^IL6 IgG Control
OT-KxPxCx^IL6 CD4/8 Depleted
L
Gastrocnemius Mass
mass (mg/g baseline BM)
OT-KxPxCx^IL6
M
Gastrocnemius Gene Expression
Sham
OT-KxPxCx^IL6 IgG
OT-KxPxCx^IL6 CD4/8
mRNA expression (fold change)
Trim63
Fbxo32

658

659 **Figure 5: CD4^{+} and CD8^{+} T cells are necessary for OT-KxPxCx^{IL6} tumor clearance**. (A-C)
660 Confirmation of CD4/CD8a T cell depletion via flow cytometry on spleen 12 days post
661 implantation for (A)CD90.2+ total T cells, (B) CD8+ T cells, (C) CD4+ T cells. (D) Survival
662 comparison of OT-KxPxCx^{IL6} mice given CD4/CD8 depletion or IgG control antibodies.
663 Statistically tested with Log-rank (Mantel-Cox) test. (E) OT-KxPxCx$^{IL6\text{-}LUC}$ tumor growth,
664 measured by IVIS imaging. Statistically tested with 2-way ANOVA, for time points with
665 representation from both groups, with Šídák multiple testing correction. (F) Representative
666 images from IVIS imaging of OT-KxPxCx$^{IL6\text{-}LUC}$ 10 minutes after luciferin injection. Images are
667 of the same animals longitudinally. CD4/CD8 depleted mice reached humane endpoint prior to
668 D10 scan. (G) Pancreas and tumor mass at endpoint. (H) Representative pancreas cross
669 sections at humane euthanasia endpoint from IgG control (top) and CD4/CD8 depleted
670 (bottom) mice. Scale bars represent 100 um. (I) expression of *Il6 transgene* expression,
671 measured by qPCR. (J) Plasma IL-6 measured by ELISA. (K) Body mass change as a
672 percentage of initial body mass over time. Statistically tested with Mixed-effects analysis with
673 repeated measures. P<0.0001 for Time and Time x Tumor Status. p=0.0048 for Tumor Status.
674 (L) Gastrocnemius muscle mass at humane euthanasia endpoint normalized to initial body
675 mass. (M) Atrophy-related gene expression (*Trim63* and *Fbxo32*) in gastrocnemius muscle,
676 measured by qPCR. All male mice, N = 5 sham, 10 KxPxCx^{IL6} per antibody treatment group.
677 Error bars represent SEM. 3 group studies were statistically tested with a 1-way ANOVA and
678 Tukey correction for multiple comparisons. **** P<0.0001, ***P<0.001, **P<0.01, *P<0.05.

679

Figure 6

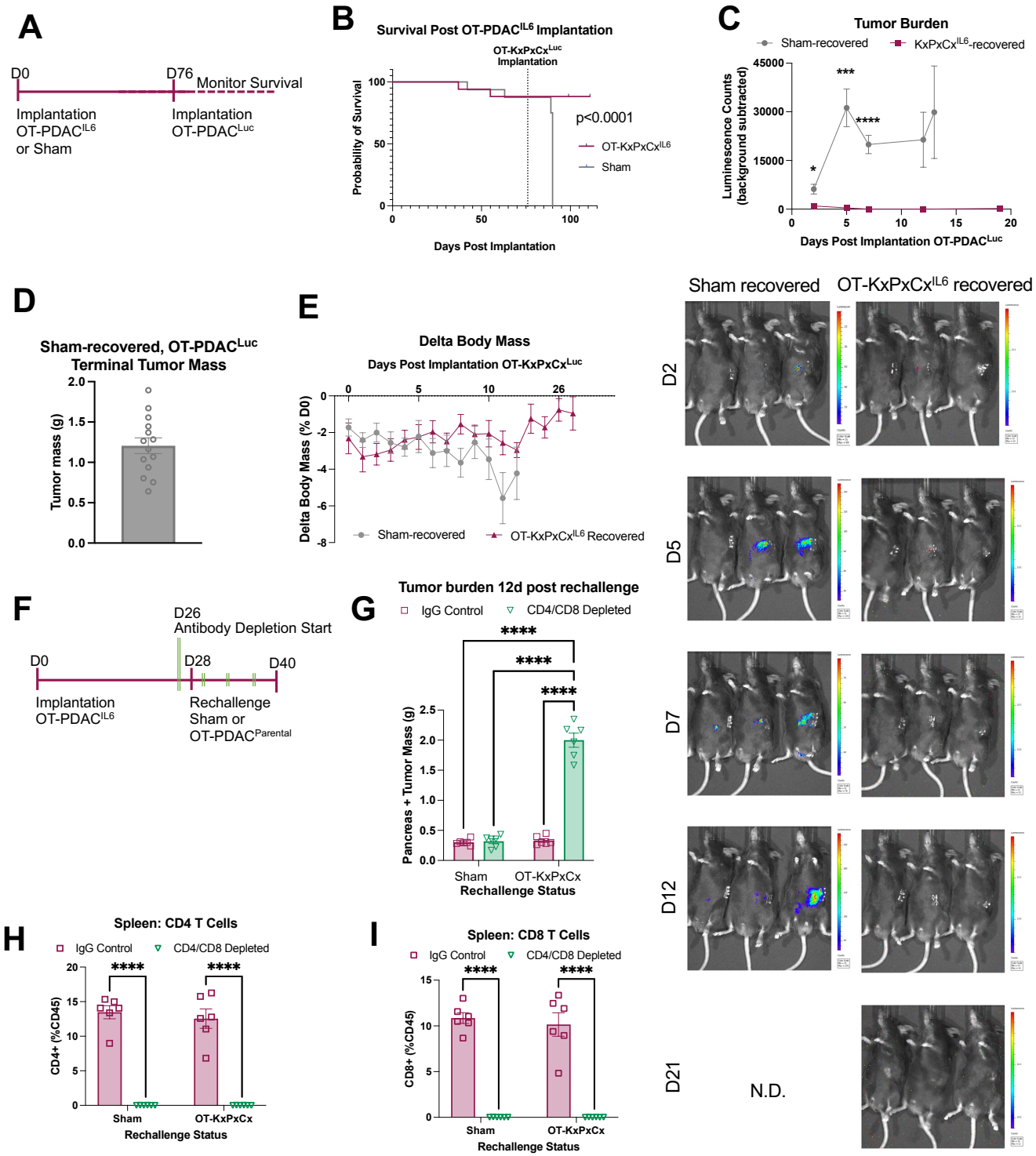
A
D0
D76
Monitor Survival
Implantation OT-PDAC^IL6 or Sham
Implantation OT-PDAC^Luc
B
Survival Post OT-PDAC^IL6 Implantation
OT-KxPxCx^Luc Implantation
Probability of Survival
p<0.0001
OT-KxPxCx^IL6
Sham
Days Post Implantation
C
Tumor Burden
Sham-recovered
KxPxCx^IL6-recovered
Luminescence Counts (background subtracted)
Days Post Implantation OT-PDAC^Luc
D
Sham-recovered, OT-PDAC^Luc Terminal Tumor Mass
Tumor mass (g)
E
Delta Body Mass
Days Post Implantation OT-KxPxCx^Luc
Delta Body Mass (% D0)
Sham-recovered
OT-KxPxCx^IL6 Recovered
Sham recovered
OT-KxPxCx^IL6 recovered
D2
D5
D7
D12
D21
N.D.
F
D26 Antibody Depletion Start
D0
D28
D40
Implantation OT-PDAC^IL6
Rechallenge Sham or OT-PDAC^Parental
G
Tumor burden 12d post rechallenge
IgG Control
CD4/CD8 Depleted
Pancreas + Tumor Mass (g)
Sham
OT-KxPxCx
Rechallenge Status
H
Spleen: CD4 T Cells
IgG Control
CD4/CD8 Depleted
CD4+ (%CD45)
Sham
OT-KxPxCx
Rechallenge Status
I
Spleen: CD8 T Cells
IgG Control
CD4/CD8 Depleted
CD8+ (%CD45)
Sham
OT-KxPxCx
Rechallenge Status

681 **Figure 6: OT-KxPxCx^{IL6} induces a durable T cell response to OT-KxPxCx^{Parental} tumors.**
682 (A) Schematic timeline for B-E. Mice were implanted with OT-KxPxCx^{IL6} or given sham
683 surgery, then all mice were rechallenged with OT-KxPxCx$^{Parental-LUC}$ after 76 days. (B) Survival
684 comparison of OT-KxPxCx^{IL6}-recovered and sham-recovered mice. Statistically tested with
685 Log-rank (Mantel-Cox) test. (C) OT-KxPxCx$^{Parental-LUC}$ tumor growth, measured by IVIS
686 imaging. Statistically tested with mixed effects model and Šídák multiple testing correction,
687 using imputation to match KxPxCx^{IL6} endpoint with the sham endpoint. Corresponding IVIS
688 images below. (D) Tumor mass at humane euthanasia endpoint for sham-recovered OT-
689 KxPxCx$^{Parental-LUC}$ tumors. (E) Body mass change as a percentage of initial body mass over
690 time. Statistically tested with mixed effects model and Šídák multiple testing correction at
691 timepoints where both groups were represented. p=0.0435 for Time, p=0.4903 for Tumor
692 Status, p=0.0002 for Time x Tumor Status. (A-E) N = 7 male KxPxCx^{IL6}, 8 male sham, 7
693 female KxPxCx^{IL6}, 6 female sham. (F) Schematic timeline for G-I. Mice were implanted with
694 OT-KxPxCx^{IL6} or given Sham surgery. 28 days later, mice were rechallenged with OT-
695 KxPxCx^{Parental}, and given CD4/CD8 depletion or IgG control antibodies beginning on D26 and
696 every 4 days thereafter (denoted with double green lines). (G) Pancreas/tumor mass at 12
697 days. (H) Intra-tumoral CD4^{+} T cells at 12 days. (I) Intra-tumoral CD8^{+} T cells at 12 days. (F-I)
698 All male mice N = 6 per group. Error bars represent SEM. 2x2 studies were statistically tested
699 with a full effects model 2-way ANOVA and Sidak multiple comparisons test. **** P<0.0001,
700 ***P<0.001, **P<0.01, *P<0.05.

701

Figure 7

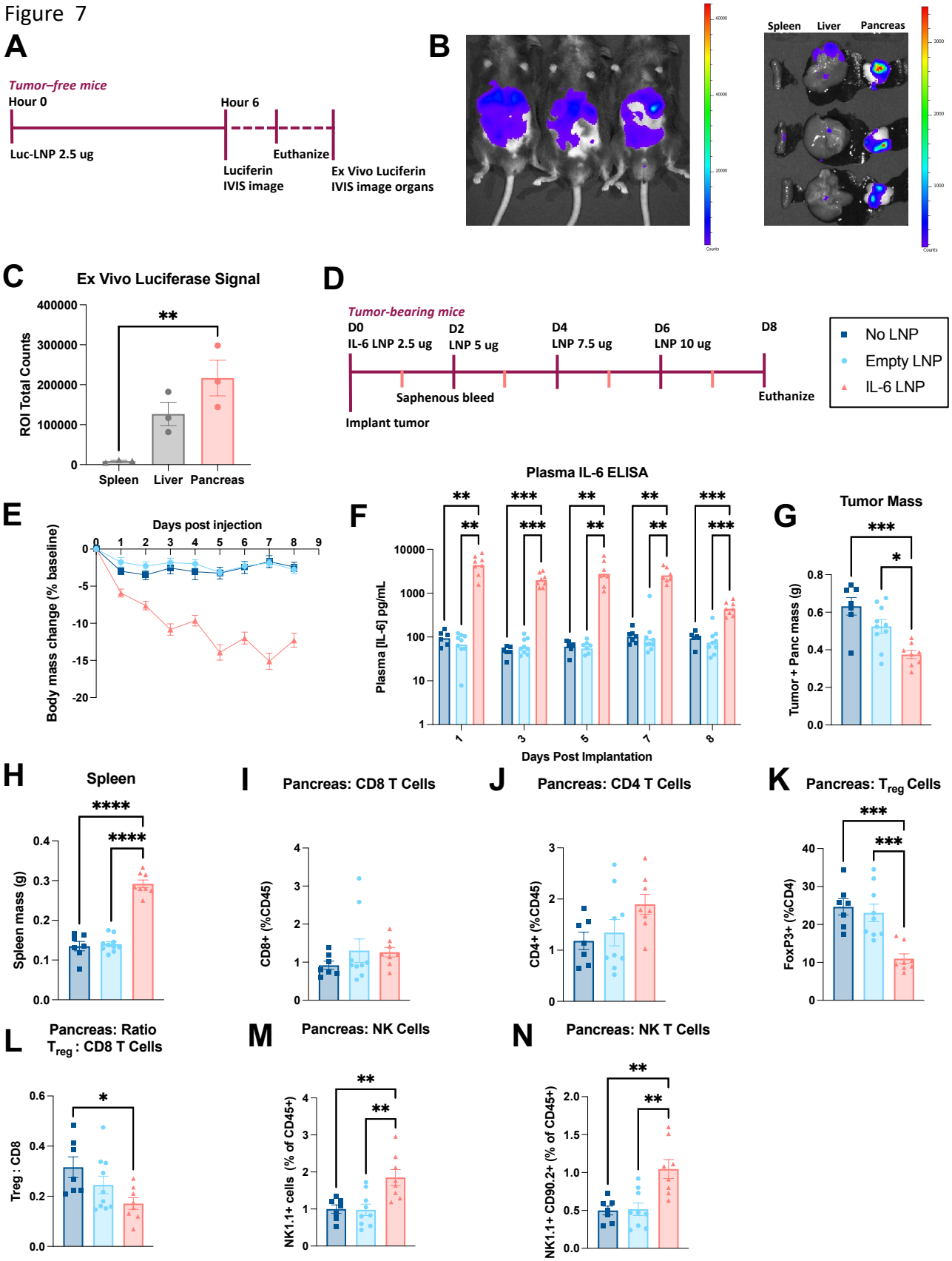
A
Tumor–free mice
Hour 0
Hour 6
Luc-LNP 2.5 ug
Luciferin
IVIS image
Euthanize
Ex Vivo Luciferin
IVIS image organs
B
Spleen
Liver
Pancreas
C
Ex Vivo Luciferase Signal
ROI Total Counts
Spleen
Liver
Pancreas
D
Tumor-bearing mice
D0
IL-6 LNP 2.5 ug
D2
LNP 5 ug
D4
LNP 7.5 ug
D6
LNP 10 ug
D8
Saphenous bleed
Implant tumor
Euthanize
No LNP
Empty LNP
IL-6 LNP
E
Days post injection
Body mass change (% baseline)
F
Plasma IL-6 ELISA
Plasma [IL-6] pg/mL
Days Post Implantation
G
Tumor Mass
Tumor + Panc mass (g)
H
Spleen
Spleen mass (g)
I
Pancreas: CD8 T Cells
CD8+ (%CD45)
J
Pancreas: CD4 T Cells
CD4+ (%CD45)
K
Pancreas: Treg Cells
FoxP3+ (%CD4)
L
Pancreas: Ratio
Treg : CD8 T Cells
Treg : CD8
M
Pancreas: NK Cells
NK1.1+ cells (% of CD45+)
N
Pancreas: NK T Cells
NK1.1+ CD90.2+ (% of CD45+)

702

703 **Figure 7: Lipid nanoparticle delivery of IL-6 mRNA replicates the anti-tumor effects**
704 **observed in OT-PDAC^{IL6}.** (A) Schematic of luciferase LNP validation. Mice were injected with
705 LNPs containing a total of 2.5 ug luciferase mRNA 6 hours prior to IVIS imaging, euthanasia,
706 tissue collection, and tissue IVIS imaging. N = 3 male mice per group. (B) left- IVIS images of
707 mice injected intraperitoneally with LNPs containing luciferase. Right – IVIS image of the
708 spleen, liver, and pancreas, incubated ex vivo with luciferin prior to imaging. (C) Comparison of
709 total luminescence counts in the pancreas and liver. Statistically tested with one-way ANOVA
710 and Tukey multiple testing correction. (D) Schematic timeline for study presented in D-N. Mice
711 were injected with LNP dose 1, 3 hours prior to tumor implantation. Mice were then injected
712 with subsequent doses on 2, 4, and 6 days post-implantation. Blood was collected by
713 saphenous bleed 1, 3, 5, and 7 days post-implantation. Mice were euthanized on day 8. N = 7
714 (No LNP), 10 (empty LNP), 8 (IL6 LNP). All mice were male. Error bars represent SEM. (E)
715 Body mass change as a percentage of initial body mass over time. Statistically tested with two-
716 way ANOVA P<0.0001 for Time, Treatment, and Time x Treatment. (F) Plasma IL-6 measured
717 by ELISA at 1, 3, 5, and 7 days post-implantation, and at euthanasia (D8). Statistically tested
718 with repeated measures mixed-effects model with Tukey correction for multiple testing. (G)
719 Tumor and pancreas mass. (H) Spleen mass. (I-N) Intra-tumoral immune cell populations from
720 pancreas: (I) $CD8^+$ T cells, (J) $CD4^+$ T cells, (K) $Foxp3^+$ T regulatory cells, (L) ratio of $Foxp3^+$ to
721 $CD8^+$ cells, representative of a the degree of anti-tumor activity in the tumor microenvironment,
722 (M) NK1.1+ NK cells, (N) NK1.1+/CD90.2+ NK T cells. 3-group analysis tested with one-way
723 ANOVA with Tukey correction for multiple testing. **** P<0.0001, ***P<0.001, **P<0.01,
724 *P<0.05.

725

726

727 **SUPPLEMENTAL INFORMATION**

Table S1: Histological assessment of transgenic tumors.

					Neutrophil Presence (Incidence)		
		Tumor Area (% total area)	Carcinoma Area (% tumor area)	Lymphoid Aggregates	<5% Tumor	5-50% Tumor	>50% Tumor
5 days	KxPxCx^{Parental}	18.75 ± 8.18	45.00 ± 13.78	2.75 ± 1.73	-	10	2
	KxPxCx^{IL6}	12.58 ± 6.79	**19.83 ± 9.96**	**12.92 ± 5.19**	-	-	12
12 days	KxPxCx^{Parental}	82.83 ± 14.43	95.83 ± 3.06	6.50 ± 3.45	4	2	-
	KxPxCx^{IL6}	**0**	NA	NA		NA	
	KxPxCx$^{CD90.1}$	75.00 ± 17.32	91.67 ± 5.85	3.50 ± 3.89	2	4	-

Values represented as mean ± SD. Bold indicates $p<0.05$ when compared to KxPxCx^{Parental}.
Day 5: Two sections per sample evaluated for neutrophil presence.

728

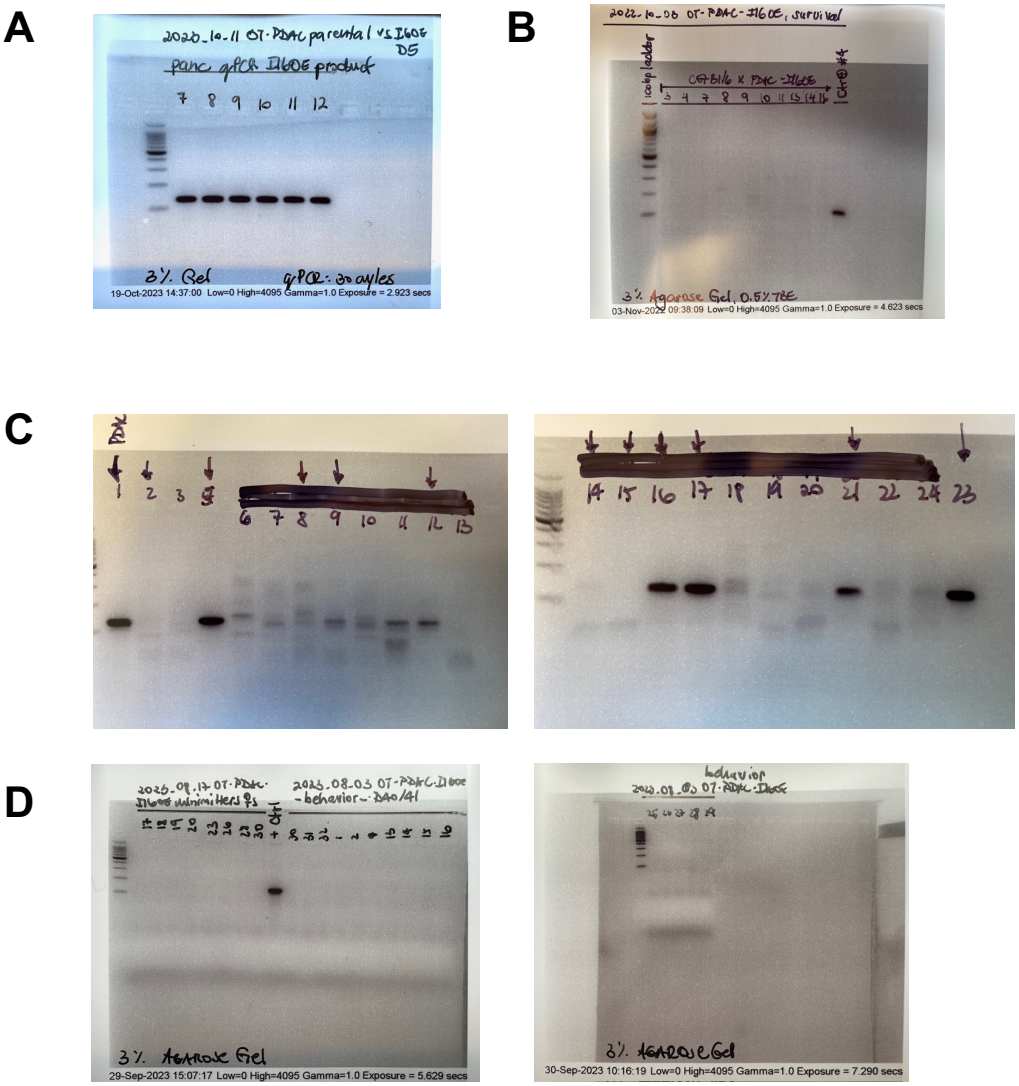

Figure S1: OT-KxPxCx^{IL6} clearance detected by *Il6-transgene* qPCR product. qPCR products from pancreas/tumor tissue, run for 30 PCR cycles, and then run out on a 3% agarose gel. Expected product is 131 bp. Ladder is Promega 100 bp ladder (G210A). (A) 5 days post implantation. (B) 17 days post implantation (samples 7, 9, 11, 16) and 24 days post implantation (samples 3, 4, 8, 10, 14). (C)10 days post implantation. (D) 40 days post implantation.

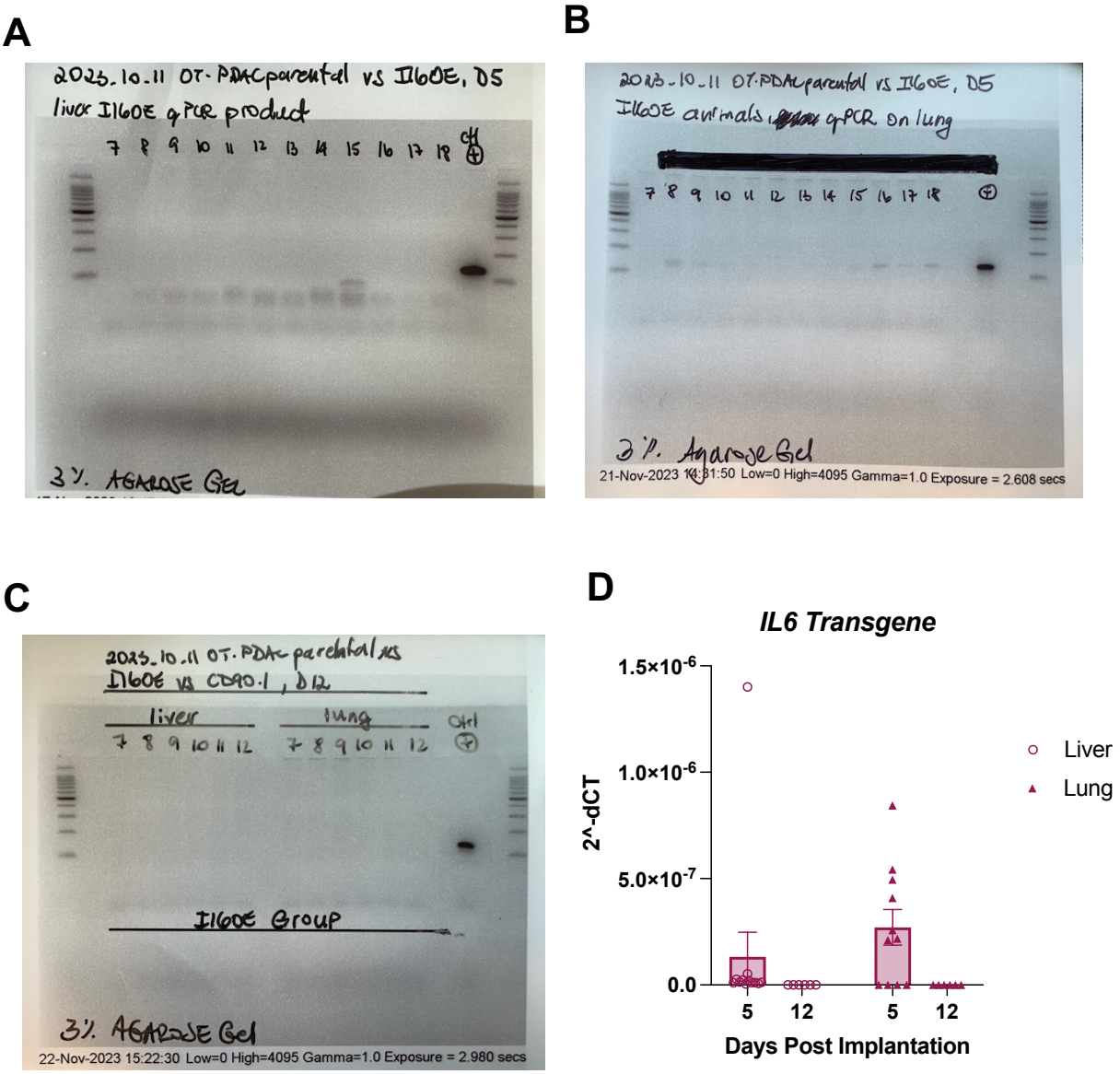

Figure S2: KxPxCx^{IL6} metastatic cell presence detected by *Il6-transgene* qPCR product. qPCR products, run for 30 PCR cycles, and then run out on a 3% agarose gel. Expected product is 131 bp. Ladder is Promega 100 bp ladder (G210A). (A) Whole liver at 5 days post implantation. (B) Whole lung at 5 days post implantation. (C) Whole lung and liver at 12 days post implantation. (D) Quantification.

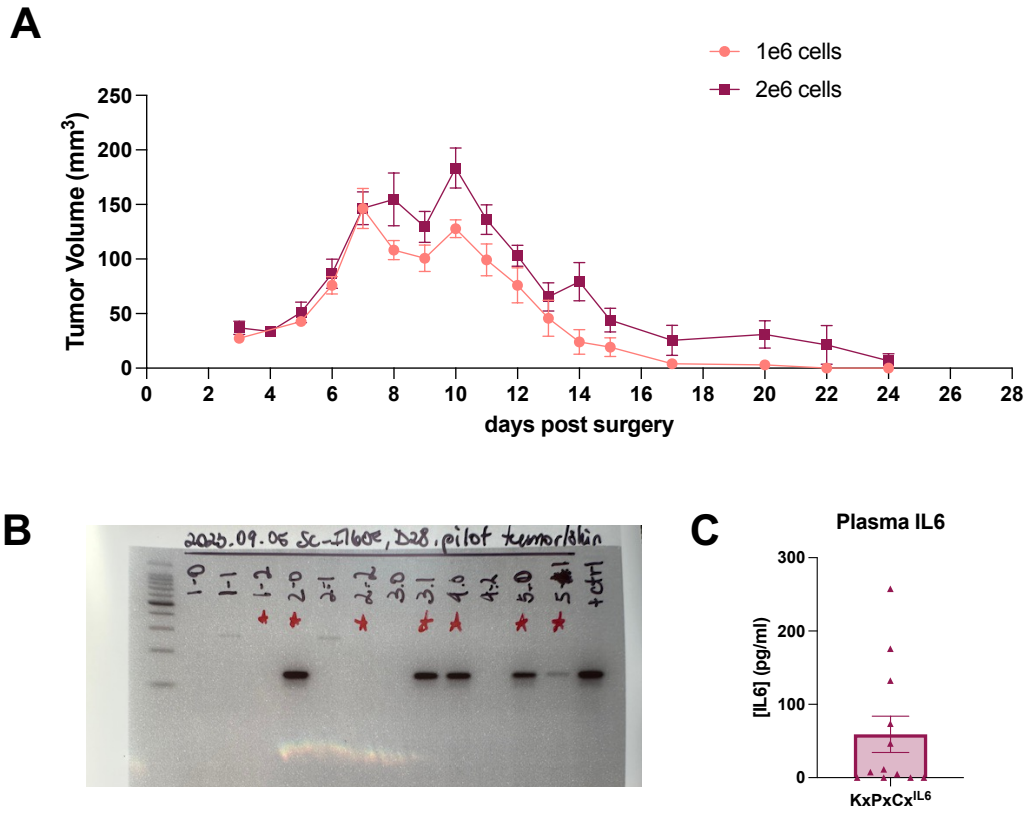

Figure S3: KxPxCx^{IL6} cells induce anti-tumor immune response when implanted subcutaneously. (A) Tumor volume measured by calipers daily. (B) Injection site/tumor tissue collected at 24 days post implantation qPCR products, run for 30 PCR cycles, and then run out on a 3% agarose gel. Expected product is 131 bp. Ladder is Promega 100 bp ladder (G210A). (C) Plasma IL-6 measured by ELISA at 24 days post implantation.

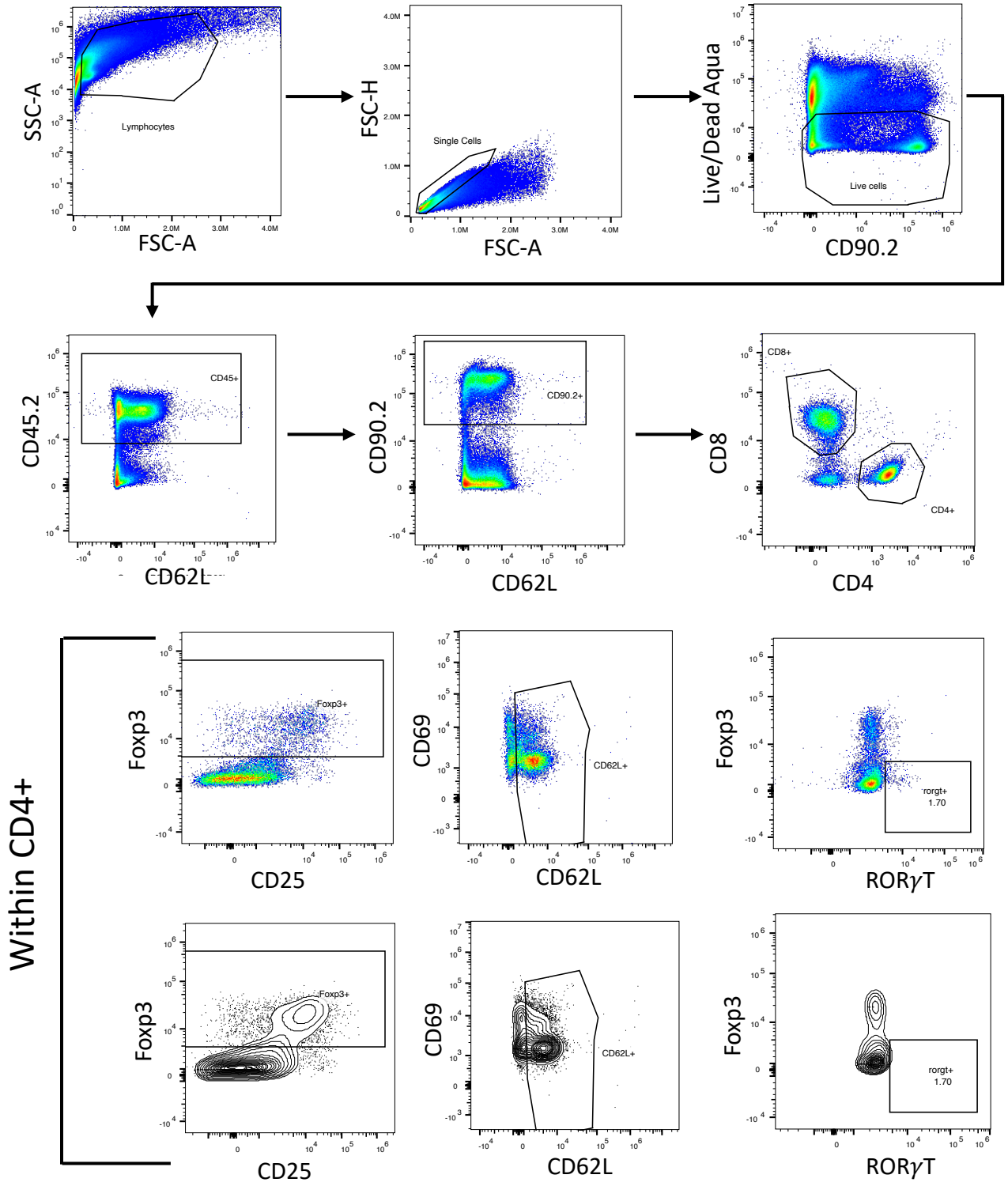

Figure S4: Gating strategy for flow cytometry presented in Figure 4B-G, and Figure S6 B-E, G (representative sample).

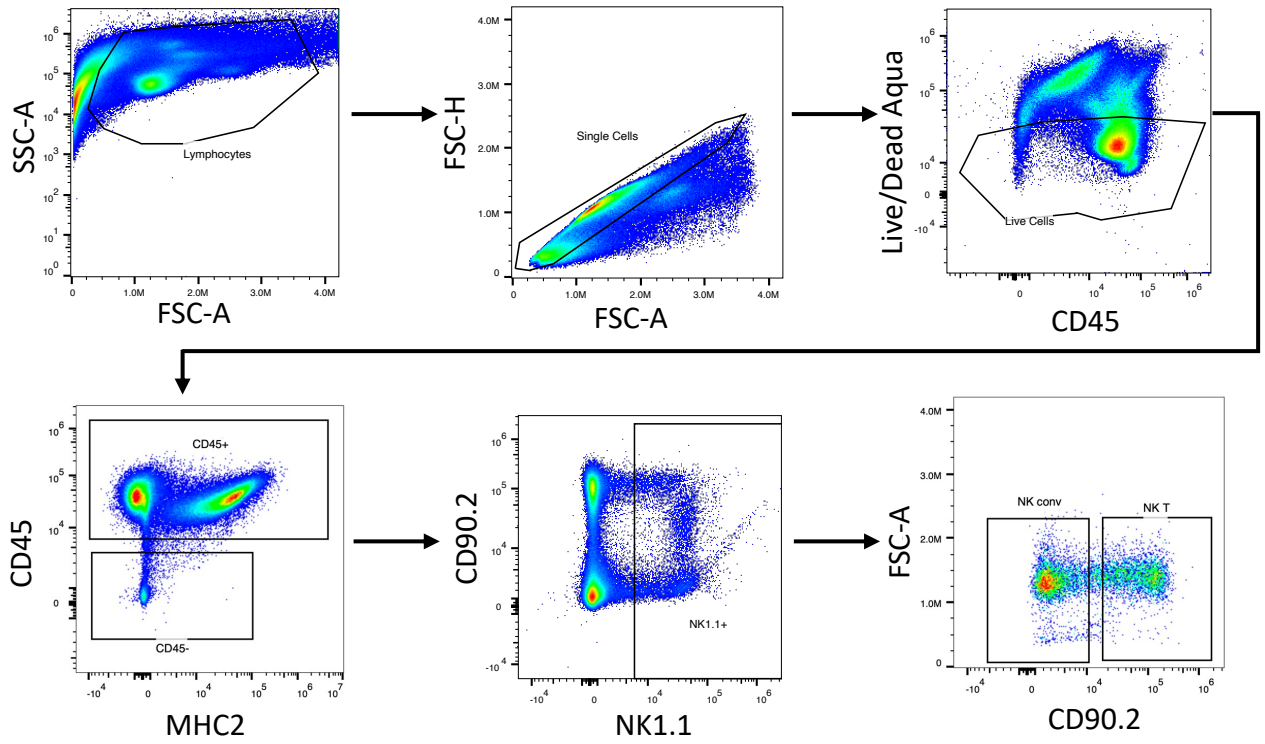

Figure S5: Gating strategies for flow cytometry presented in Figure 4H-I, and Figure S6A, F (representative sample).

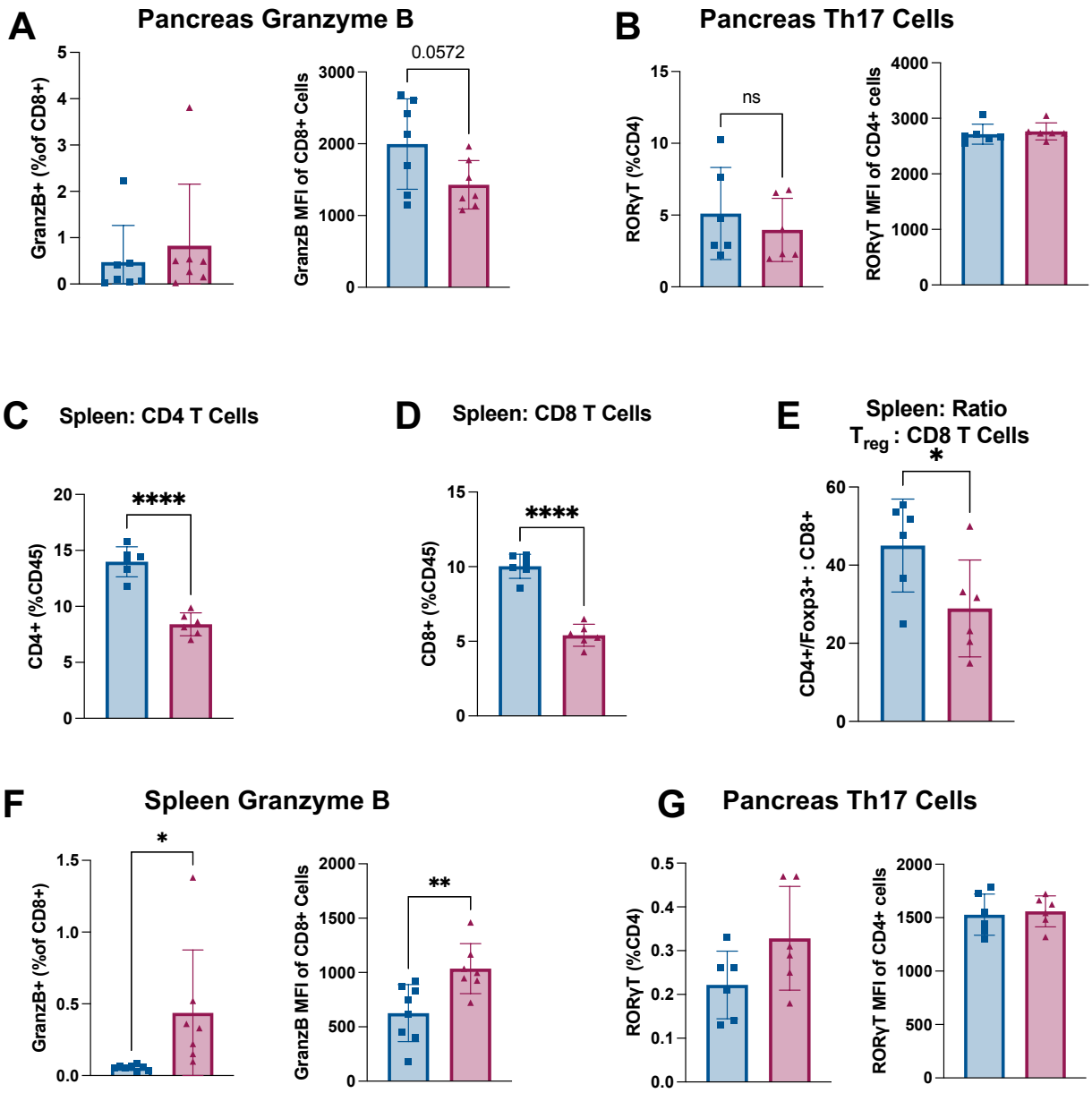

Figure S6: Supporting flow cytometry data for Th17 and Granzyme B+ T cell phenotypes. Intra-tumoral immune cell populations from pancreas at 5 days: (A) Granzyme B+ cells as a percent of CD8+ cells (left) and CD8+ Granzyme B MFI (right). (B) Th17 Cells (RORγT+) as a percent of CD4+ cells (left) and CD4+ RORγT MFI (right). Immune cell populations from spleen at 5 days: (C) CD4$^+$ T cells, (D) CD8$^+$ T cells, (E) Ratio of Foxp3$^+$ to CD8$^+$ cells, (F) Granzyme B+ cells as a percent of CD8+ cells (left) and CD8+ Granzyme B MFI (right). (G) Th17 Cells (RORγT+) as a percent of CD4+ cells (left) and CD4+ RORγT MFI (right). (B-E, G) N = 6 male mice per group. (A, F) N = 4 female, 3 male mice per group. Error bars represent SEM. 2-group analysis tested with unpaired t-test. **** $p<0.0001$, ***$p<0.001$, **$p<0.01$, *$p<0.05$.

734

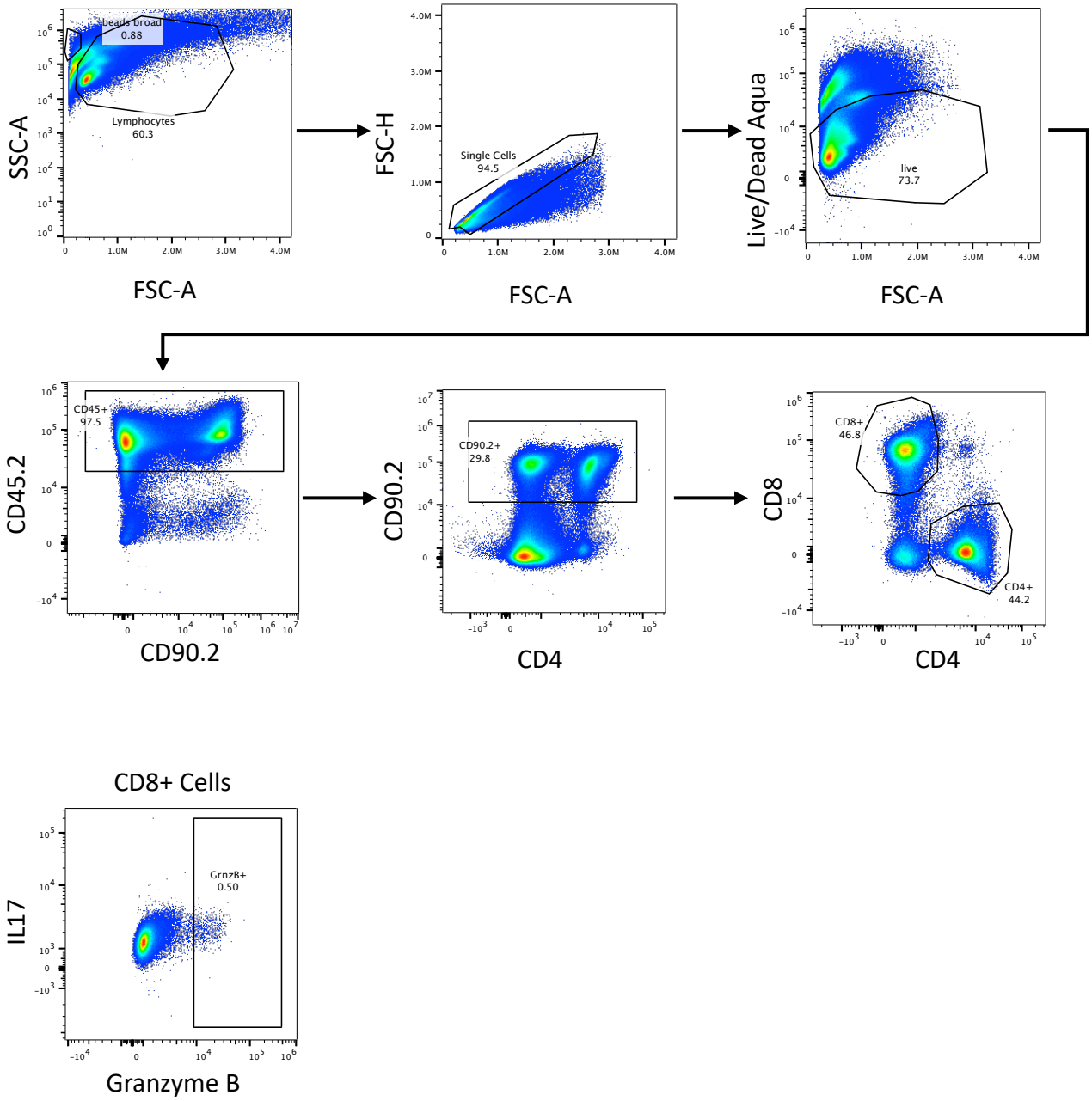

Figure S7: Granzyme B gating strategy for flow cytometry presented in Figure S6 (representative samples).

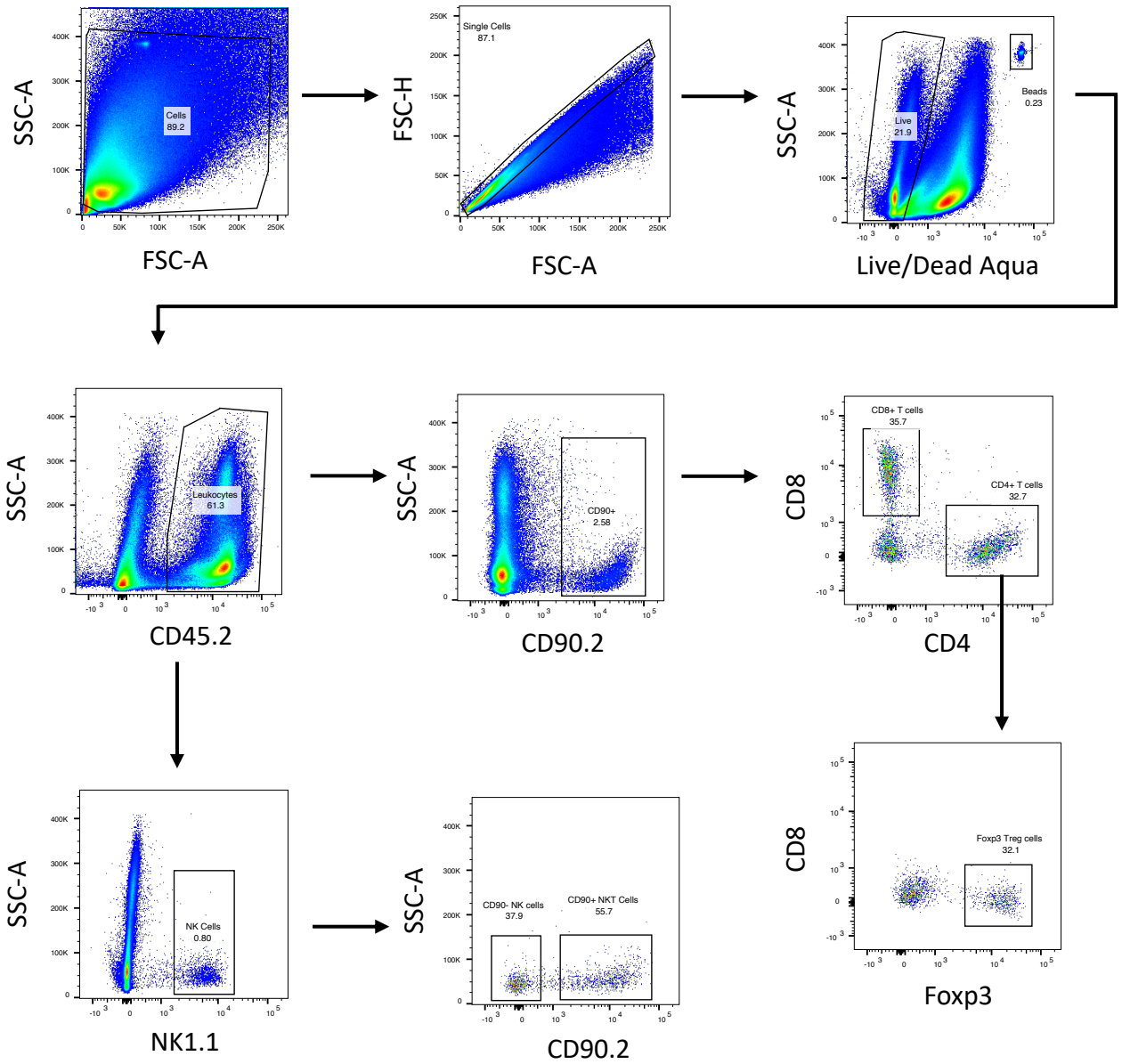

Figure S8: Gating strategies for flow cytometry presented in Figure 7 (representative sample).

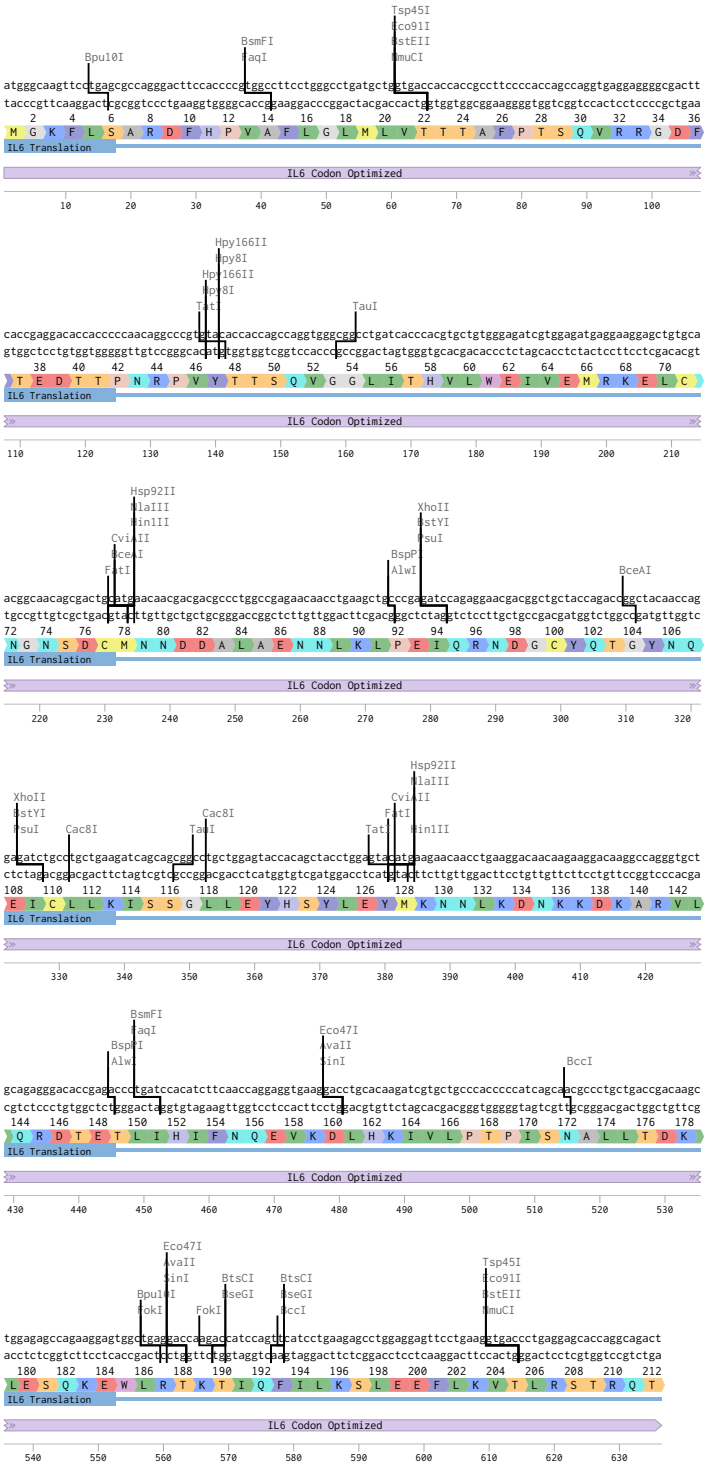

Figure S9: Linear sequence map with amino acid annotation for codon-optimized IL6 overexpression cassette transduced into PDAC cells.

Table S2: qPCR primer and probe information

Gene Name	**Supplier**	**Cat. Number**
18S	Thermo	4333760F
Fbxo32	IDT	Mm.PT.58.7025875
Trim63	IDT	Mm.PT.58.32840172
Il6-transgene	IDT	F: CGTGGAGATGAGGAAGGAGC R: GGTTGTAGCCGGTCTGGTAG

Table S3: Flow cytometry antibody information

Protein (clone)	**Host**	**Target**	**Supplier**	**Cat. Number**	**Use**
CD3 (17A2)	Rat	Mouse	Biolegend	100209	Tissue staining
CD4 (RM4-5)	Rat	Mouse	BD Pharmingen	561115	Flow
CD45.2 (104)	Mouse	Mouse	BD Horizon	563686	Flow
CD62L (MEL-14)	Rat	Mouse	BD Pharmingen	5**605**14	Flow
CD8 (53-6.7)	Rat	Mouse	BD Pharmingen	557959	Flow
CD90.2 (53-2.1)	Mouse	Mouse	BD Pharmingen	553004	Flow
FoxP3 (FJK-16s)	Rat	Mouse	eBioscience (ThermoFisher)	12-5773-82	Flow
Granzyme B (GB11)	Mouse	Mouse	Biolegend	515403	Flow
NK1.1 (PK136)	Mouse	Mouse	BD Pharmingen	552878	Flow
PanCK (AE1/AE3)	Mouse	Mouse	eBioscience (ThermoFisher)	53-9003-82	Tissue staining
RORγT (AFKJS-9)	Rat	Mouse	eBioscience (ThermoFisher)	17-6988-82	Flow

739

740 **REFERENCES**

741 1. Winograd R, Byrne KT, Evans RA, et al. Induction of T-cell immunity overcomes
742 complete resistance to PD-1 and CTLA-4 blockade and improves survival in pancreatic
743 carcinoma. Cancer immunology research 2015;3:399-411.
744 2. Beatty GL, Eghbali S, Kim R. Deploying immunotherapy in pancreatic cancer: defining
745 mechanisms of response and resistance. American Society of Clinical Oncology
746 Educational Book 2017;37:267-278.
747 3. Aznar MA, Good CR, Barber-Rotenberg JS, et al. Clinical and molecular dissection of
748 CAR T cell resistance in pancreatic cancer. Cell Reports Medicine 2025.
749 4. Byrne KT, Vonderheide RH. CD40 stimulation obviates innate sensors and drives T cell
750 immunity in cancer. Cell reports 2016;15:2719-2732.
751 5. Gnerlich JL, Mitchem JB, Weir JS, et al. Induction of Th17 cells in the tumor
752 microenvironment improves survival in a murine model of pancreatic cancer. The
753 Journal of Immunology 2010;185:4063-4071.
754 6. Delvecchio FR, Fincham RE, Spear S, et al. Pancreatic cancer chemotherapy is
755 potentiated by induction of tertiary lymphoid structures in mice. Cellular and Molecular
756 Gastroenterology and Hepatology 2021;12:1543-1565.
757 7. Hotz C, Wagenaar TR, Gieseke F, et al. Local delivery of mRNA-encoded cytokines
758 promotes antitumor immunity and tumor eradication across multiple preclinical tumor
759 models. Science translational medicine 2021;13:eabc7804.
760 8. Corcoran RB, Contino G, Deshpande V, et al. STAT3 plays a critical role in KRAS-
761 induced pancreatic tumorigenesis. Cancer research 2011;71:5020-5029.

762 9. Suh S-Y, Choi YS, Yeom CH, et al. Interleukin-6 but not tumour necrosis factor-alpha
763 predicts survival in patients with advanced cancer. Supportive Care in Cancer
764 2013;21:3071-3077.
765 10. Rupert JE, Narasimhan A, Jengelley DH, et al. Tumor-derived IL-6 and trans-signaling
766 among tumor, fat, and muscle mediate pancreatic cancer cachexia. Journal of
767 Experimental Medicine 2021;218:e20190450.
768 11. Razidlo GL, Burton KM, McNiven MA. Interleukin-6 promotes pancreatic cancer cell
769 migration by rapidly activating the small GTPase CDC42. Journal of Biological
770 Chemistry 2018;293:11143-11153.
771 12. Arneson-Wissink PC, Mendez H, Pelz K, et al. Hepatic signal transducer and activator
772 of transcription-3 signalling drives early-stage pancreatic cancer cachexia via
773 suppressed ketogenesis. Journal of Cachexia, Sarcopenia and Muscle 2024.
774 13. Flint TR, Janowitz T, Connell CM, et al. Tumor-induced IL-6 reprograms host
775 metabolism to suppress anti-tumor immunity. Cell metabolism 2016;24:672-684.
776 14. Zhang Y, Yan W, Collins MA, et al. Interleukin-6 is required for pancreatic cancer
777 progression by promoting MAPK signaling activation and oxidative stress resistance.
778 Cancer research 2013;73:6359-6374.
779 15. Fujimoto M, Nakano M, Terabe F, et al. The influence of excessive IL-6 production in
780 vivo on the development and function of Foxp3+ regulatory T cells. The Journal of
781 Immunology 2011;186:32-40.
782 16. Jiang Z, Liao R, Lv J, et al. IL-6 trans-signaling promotes the expansion and anti-tumor
783 activity of CAR T cells. Leukemia 2021;35:1380-1391.

784 17. Nejad EB, Labrie C, van Elsas MJ, et al. IL-6 signaling in macrophages is required for
785 immunotherapy-driven regression of tumors. Journal for ImmunoTherapy of Cancer
786 2021;9:e002460.
787 18. Foley K, Rucki AA, Xiao Q, et al. Semaphorin 3D autocrine signaling mediates the
788 metastatic role of annexin A2 in pancreatic cancer. Science signaling 2015;8:ra77-ra77.
789 19. Quaranta V, Rainer C, Nielsen SR, et al. Macrophage-derived granulin drives resistance
790 to immune checkpoint inhibition in metastatic pancreatic cancer. Cancer research
791 2018;78:4253-4269.
792 20. Ireland L, Santos A, Ahmed MS, et al. Chemoresistance in pancreatic cancer is driven
793 by stroma-derived insulin-like growth factors. Cancer research 2016;76:6851-6863.
794 21. Ino Y, Yamazaki-Itoh R, Shimada K, et al. Immune cell infiltration as an indicator of the
795 immune microenvironment of pancreatic cancer. British journal of cancer 2013;108:914-
796 923.
797 22. Hiraoka N, Ino Y, Yamazaki-Itoh R, et al. Intratumoral tertiary lymphoid organ is a
798 favourable prognosticator in patients with pancreatic cancer. British journal of cancer
799 2015;112:1782-1790.
800 23. Sautès-Fridman C, Petitprez F, Calderaro J, et al. Tertiary lymphoid structures in the
801 era of cancer immunotherapy. Nature Reviews Cancer 2019;19:307-325.
802 24. Siegel RL, Miller KD, Wagle NS, et al. Cancer statistics, 2023. CA: a cancer journal for
803 clinicians 2023;73:17-48.
804 25. Hilmi M, Delaye M, Muzzolini M, et al. The immunological landscape in pancreatic
805 ductal adenocarcinoma and overcoming resistance to immunotherapy. The Lancet
806 Gastroenterology & Hepatology 2023.

807 26. Mace TA, Shakya R, Pitarresi JR, et al. IL-6 and PD-L1 antibody blockade combination
808 therapy reduces tumour progression in murine models of pancreatic cancer. Gut
809 2018;67:320-332.
810 27. Ware MB, Phillips M, McQuinn C, et al. Dual IL-6 and CTLA-4 blockade regresses
811 pancreatic tumors in a T cell–and CXCR3-dependent manner. JCI insight
812 2023;8:e155006.
813 28. Arneson-Wissink PC, Mendez H, Pelz K, et al. Hepatic signal transducer and activator
814 of transcription-3 signalling drives early-stage pancreatic cancer cachexia via
815 suppressed ketogenesis. J Cachexia Sarcopenia Muscle 2024;15:975-988.
816 29. Soler MF, Abaurrea A, Azcoaga P, et al. New perspectives in cancer immunotherapy:
817 targeting IL-6 cytokine family. Journal for ImmunoTherapy of Cancer 2023;11.
818 30. Lee JW, Stone ML, Porrett PM, et al. Hepatocytes direct the formation of a pro-
819 metastatic niche in the liver. Nature 2019;567:249-252.
820 31. Robinson E, MacDonald KD, Slaughter K, et al. Lipid nanoparticle-delivered chemically
821 modified mRNA restores chloride secretion in cystic fibrosis. Molecular Therapy
822 2018;26:2034-2046.
823 32. Lokugamage MP, Vanover D, Beyersdorf J, et al. Optimization of lipid nanoparticles for
824 the delivery of nebulized therapeutic mRNA to the lungs. Nature biomedical engineering
825 2021;5:1059-1068.
826 33. Flamini V, Ghadiali RS, Antczak P, et al. The satellite cell niche regulates the balance
827 between myoblast differentiation and self-renewal via p53. Stem Cell Reports
828 2018;10:970-983.

829 34. Melamed JR, Yerneni SS, Arral ML, et al. Ionizable lipid nanoparticles deliver mRNA to
830 pancreatic β cells via macrophage-mediated gene transfer. Science Advances
831 2023;9:eade1444.
832 35. Zhu Q, Yu C, Chen Y, et al. Dual mRNA nanoparticles strategy for enhanced pancreatic
833 cancer treatment and β-elemene combination therapy. Proceedings of the National
834 Academy of Sciences 2025;122:e2418306122.
835 36. Sahel DK, Renner J, Vlasova KY, et al. Improved localized mRNA delivery using lipid
836 nanoparticles with a novel synthetic cholesterol derivative. RSC pharmaceutics 2026.
837 37. Qiu X, Yang Y, Ma Q, et al. Thioketal-Incorporated Biodegradable Lipid Nanoparticles
838 Deliver mRNA to Ductal Epithelial Cells for Improved Pancreatic Cancer Treatment.
839 Journal of the American Chemical Society 2025.
840 38. Shen Q, Liu J, Zeng L, et al. Pancreas-targeted lipid nanoparticles for relatively non-
841 invasive interleukin-12 mRNA therapy in orthotopic pancreatic ductal adenocarcinoma.
842 Journal of Controlled Release 2025;381:113588.
843 39. Michaelis KA, Zhu X, Burfeind KG, et al. Establishment and characterization of a novel
844 murine model of pancreatic cancer cachexia. Journal of cachexia, sarcopenia and
845 muscle 2017;8:824-838.
846 40. Eil R, Vodnala SK, Clever D, et al. Ionic immune suppression within the tumour
847 microenvironment limits T cell effector function. Nature 2016;537:539-543.
848 41. Liu F, Whitton JL. Cutting edge: re-evaluating the in vivo cytokine responses of CD8+ T
849 cells during primary and secondary viral infections. The Journal of Immunology
850 2005;174:5936-5940.
851

Figure 1

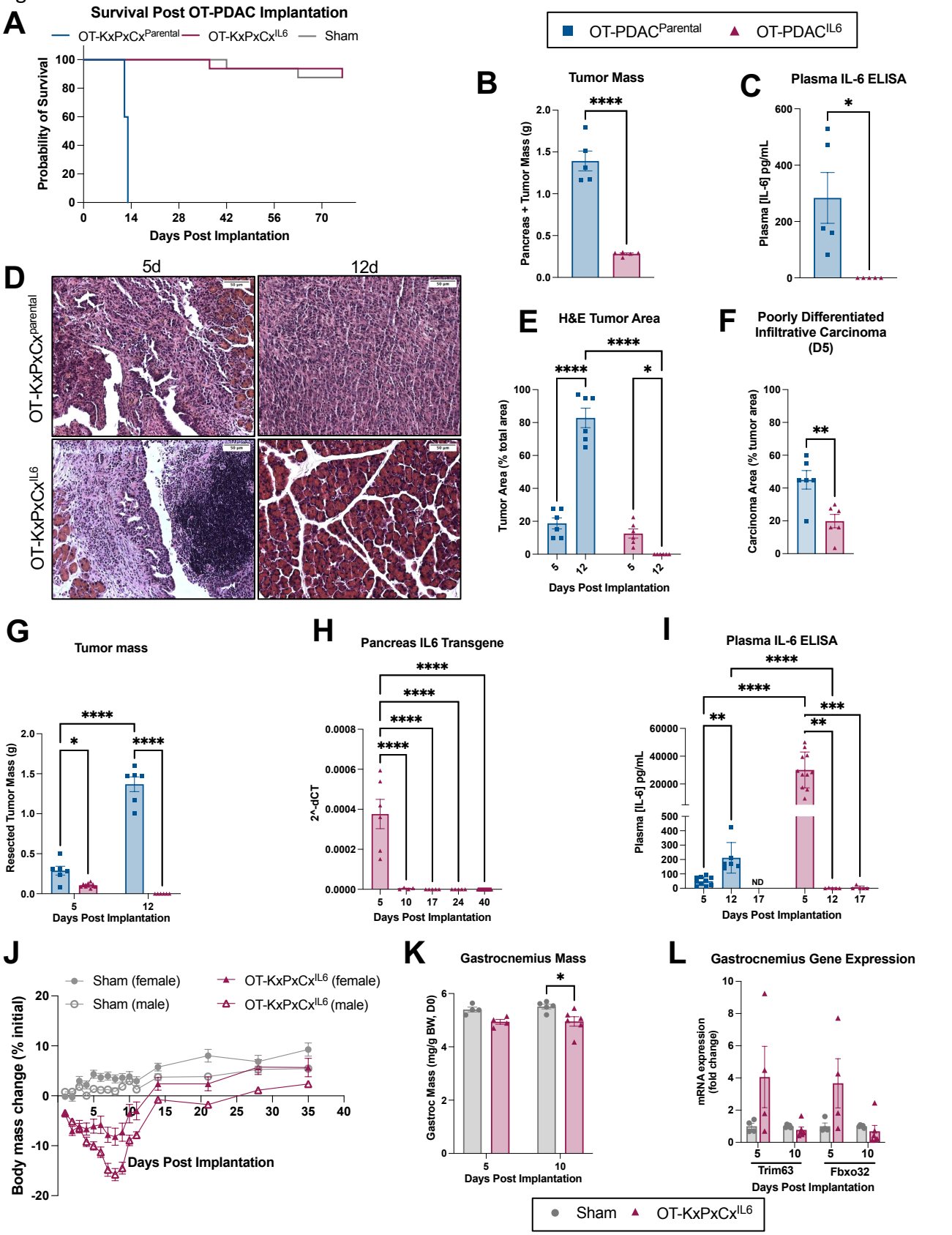
A
Survival Post OT-PDAC Implantation
OT-KxPxCx^Parental
OT-KxPxCx^IL6
Sham
Probability of Survival
Days Post Implantation
OT-PDAC^Parental
OT-PDAC^IL6
B
Tumor Mass
Pancreas + Tumor Mass (g)
C
Plasma IL-6 ELISA
Plasma [IL-6] pg/mL
D
5d
12d
OT-KxPxCx^parental
OT-KxPxCx^IL6
E
H&E Tumor Area
Tumor Area (% total area)
Days Post Implantation
F
Poorly Differentiated Infiltrative Carcinoma (D5)
Carcinoma Area (% tumor area)
G
Tumor mass
Resected Tumor Mass (g)
Days Post Implantation
H
Pancreas IL6 Transgene
2^-dCT
Days Post Implantation
I
Plasma IL-6 ELISA
Plasma [IL-6] pg/mL
ND
Days Post Implantation
J
Sham (female)
Sham (male)
OT-KxPxCx^IL6 (female)
OT-KxPxCx^IL6 (male)
Body mass change (% initial)
Days Post Implantation
K
Gastrocnemius Mass
Gastroc Mass (mg/g BW, D0)
Days Post Implantation
L
Gastrocnemius Gene Expression
mRNA expression (fold change)
Trim63
Fbxo32
Days Post Implantation
Sham
OT-KxPxCx^IL6

Figure 2

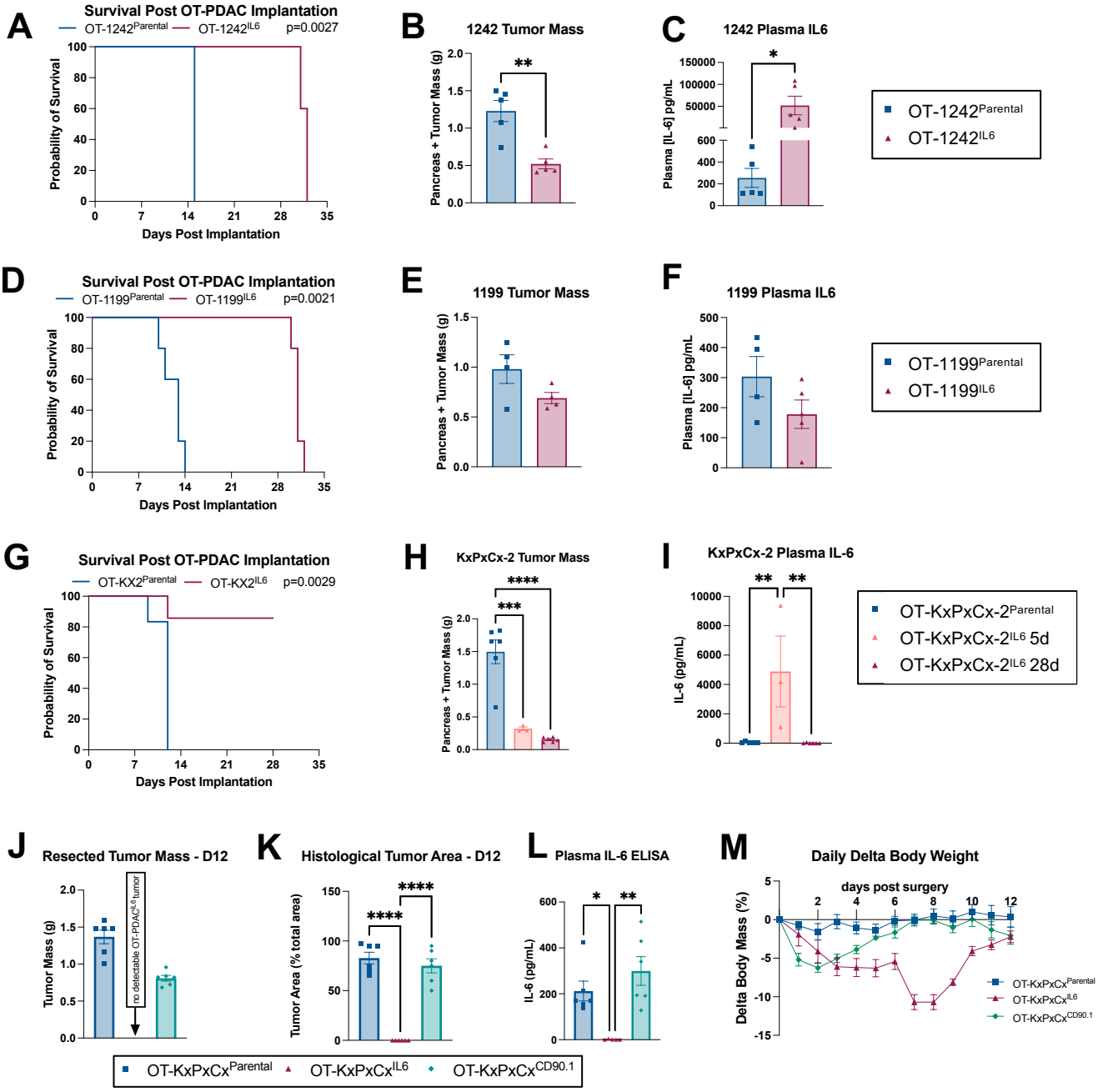
A
Survival Post OT-PDAC Implantation
OT-1242Parental
OT-1242IL6
p=0.0027
Probability of Survival
Days Post Implantation
B
1242 Tumor Mass
Pancreas + Tumor Mass (g)
**
C
1242 Plasma IL6
Plasma [IL-6] pg/mL
*
OT-1242Parental
OT-1242IL6
D
Survival Post OT-PDAC Implantation
OT-1199Parental
OT-1199IL6
p=0.0021
Probability of Survival
Days Post Implantation
E
1199 Tumor Mass
Pancreas + Tumor Mass (g)
F
1199 Plasma IL6
Plasma [IL-6] pg/mL
OT-1199Parental
OT-1199IL6
G
Survival Post OT-PDAC Implantation
OT-KX2Parental
OT-KX2IL6
p=0.0029
Probability of Survival
Days Post Implantation
H
KxPxCx-2 Tumor Mass
Pancreas + Tumor Mass (g)
****
***
I
KxPxCx-2 Plasma IL-6
IL-6 (pg/mL)
**
**
OT-KxPxCx-2Parental
OT-KxPxCx-2IL6 5d
OT-KxPxCx-2IL6 28d
J
Resected Tumor Mass - D12
Tumor Mass (g)
no detectable OT-PDACIL6 tumor
K
Histological Tumor Area - D12
Tumor Area (% total area)
****
****
L
Plasma IL-6 ELISA
IL-6 (pg/mL)
*
**
M
Daily Delta Body Weight
days post surgery
Delta Body Mass (%)
OT-KxPxCxParental
OT-KxPxCxIL6
OT-KxPxCxCD90.1
OT-KxPxCxParental
OT-KxPxCxIL6
OT-KxPxCxCD90.1

Figure 3

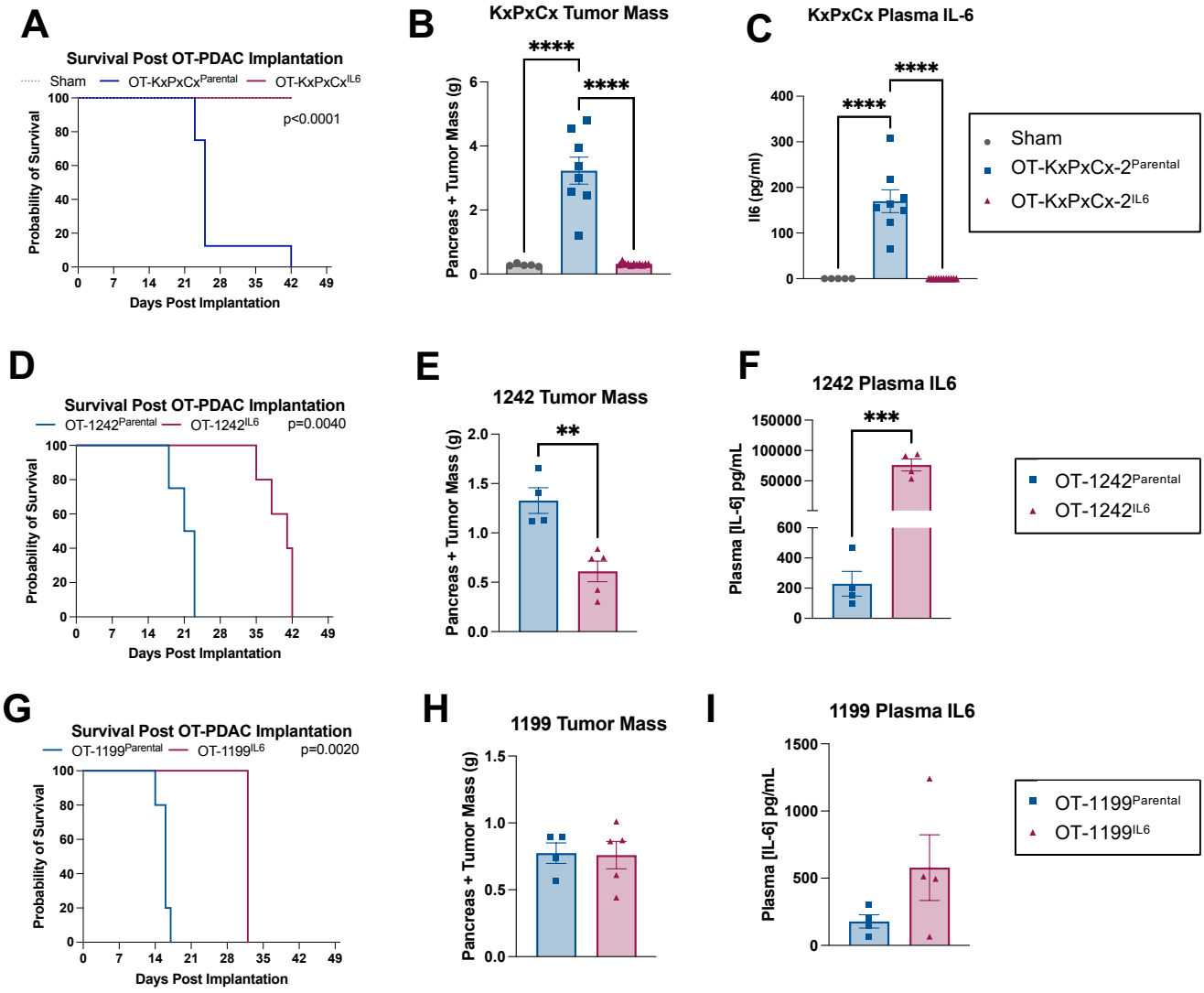
A
Survival Post OT-PDAC Implantation
Sham
OT-KxPxCx^Parental
OT-KxPxCx^IL6
p<0.0001
Probability of Survival
Days Post Implantation
B
KxPxCx Tumor Mass
****
****
Pancreas + Tumor Mass (g)
C
KxPxCx Plasma IL-6
****
****
Il6 (pg/ml)
Sham
OT-KxPxCx-2^Parental
OT-KxPxCx-2^IL6
D
Survival Post OT-PDAC Implantation
OT-1242^Parental
OT-1242^IL6
p=0.0040
Probability of Survival
Days Post Implantation
E
1242 Tumor Mass
**
Pancreas + Tumor Mass (g)
F
1242 Plasma IL6
***
Plasma [IL-6] pg/mL
OT-1242^Parental
OT-1242^IL6
G
Survival Post OT-PDAC Implantation
OT-1199^Parental
OT-1199^IL6
p=0.0020
Probability of Survival
Days Post Implantation
H
1199 Tumor Mass
Pancreas + Tumor Mass (g)
I
1199 Plasma IL6
Plasma [IL-6] pg/mL
OT-1199^Parental
OT-1199^IL6

Figure 4

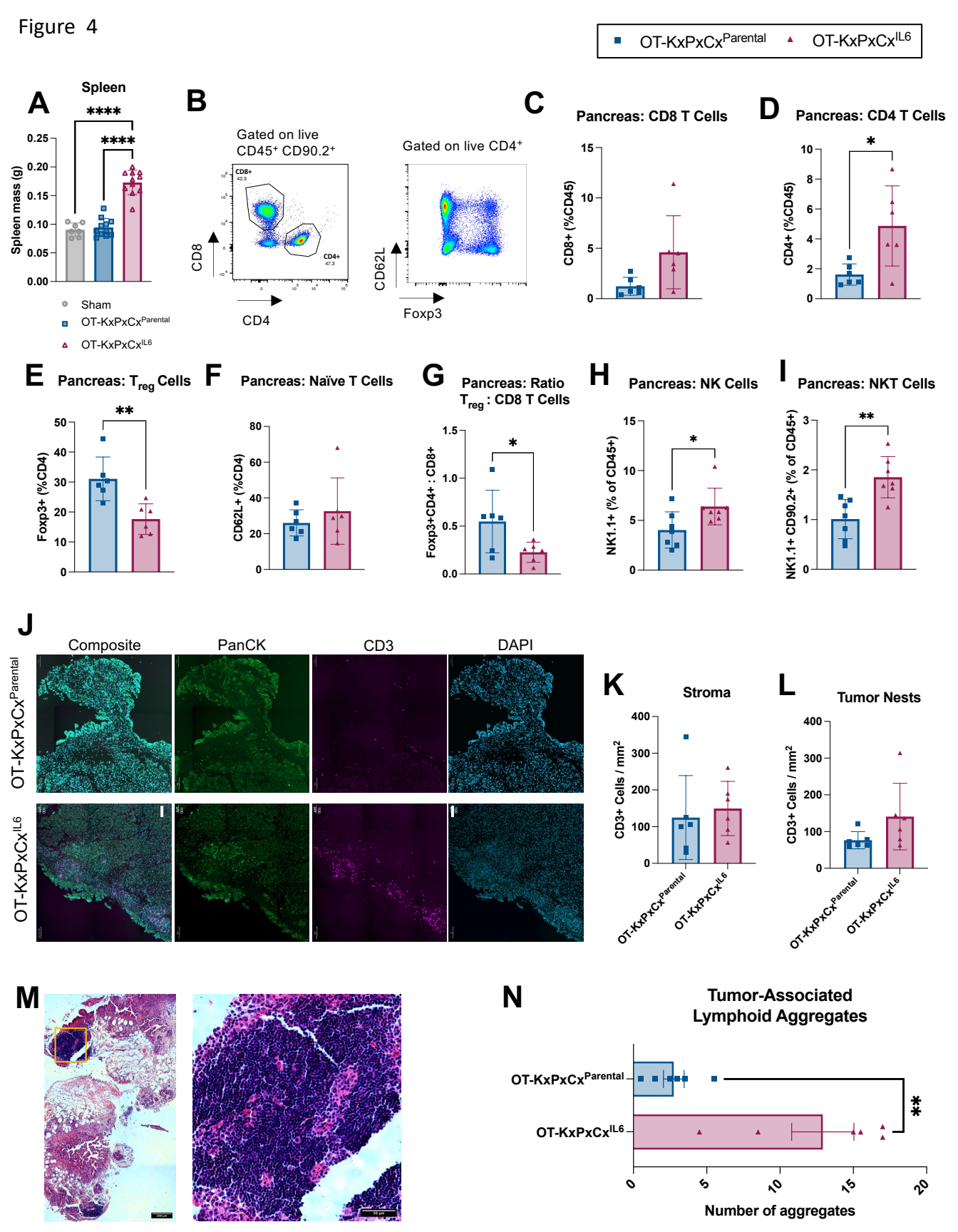
OT-KxPxCx^Parental
OT-KxPxCx^IL6
A
Spleen
****
****
Spleen mass (g)
0.25
0.20
0.15
0.10
0.05
0.00
Sham
OT-KxPxCx^Parental
OT-KxPxCx^IL6
B
Gated on live CD45+ CD90.2+
CD8+
42.3
CD4+
47.3
CD8
CD4
Gated on live CD4+
CD62L
Foxp3
C
Pancreas: CD8 T Cells
CD8+ (%CD45)
D
Pancreas: CD4 T Cells
*
CD4+ (%CD45)
E
Pancreas: Treg Cells
**
Foxp3+ (%CD4)
F
Pancreas: Naïve T Cells
CD62L+ (%CD4)
G
Pancreas: Ratio Treg : CD8 T Cells
*
Foxp3+CD4+ : CD8+
H
Pancreas: NK Cells
*
NK1.1+ (% of CD45+)
I
Pancreas: NKT Cells
**
NK1.1+ CD90.2+ (% of CD45+)
J
Composite
PanCK
CD3
DAPI
OT-KxPxCx^Parental
OT-KxPxCx^IL6
K
Stroma
CD3+ Cells / mm2
OT-KxPxCx^Parental
OT-KxPxCx^IL6
L
Tumor Nests
CD3+ Cells / mm2
OT-KxPxCx^Parental
OT-KxPxCx^IL6
M
N
Tumor-Associated Lymphoid Aggregates
OT-KxPxCx^Parental
OT-KxPxCx^IL6
**
0
5
10
15
20
Number of aggregates

Figure 5

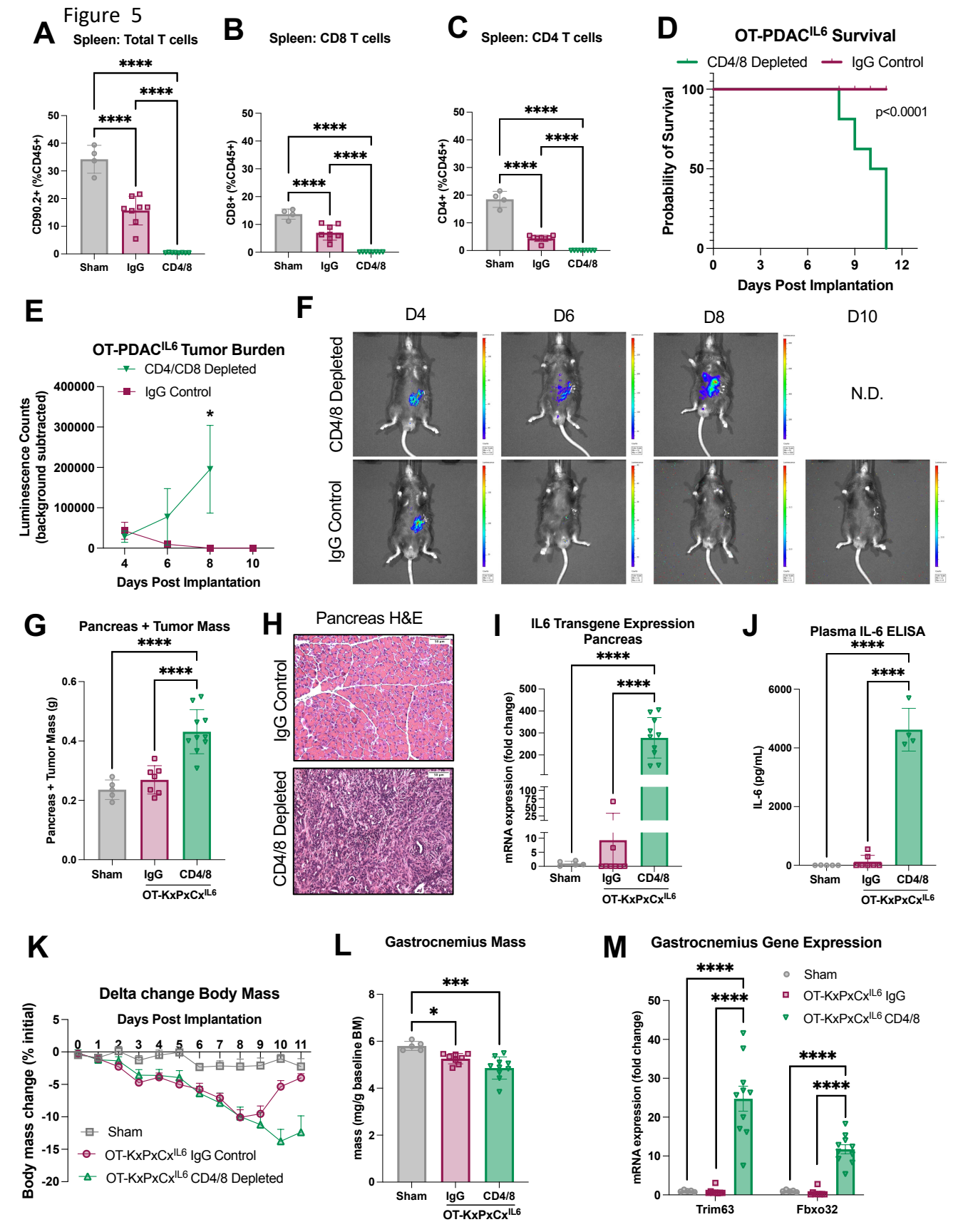
A
Spleen: Total T cells
CD90.2+ (%CD45+)
Sham
IgG
CD4/8
B
Spleen: CD8 T cells
CD8+ (%CD45+)
C
Spleen: CD4 T cells
CD4+ (%CD45+)
D
OT-PDAC^{IL6} Survival
CD4/8 Depleted
IgG Control
p<0.0001
Probability of Survival
Days Post Implantation
E
OT-PDAC^{IL6} Tumor Burden
CD4/CD8 Depleted
IgG Control
Luminescence Counts (background subtracted)
Days Post Implantation
F
D4
D6
D8
D10
CD4/8 Depleted
IgG Control
N.D.
G
Pancreas + Tumor Mass
Pancreas + Tumor Mass (g)
OT-KxPxCx^{IL6}
H
Pancreas H&E
IgG Control
CD4/8 Depleted
I
IL6 Transgene Expression Pancreas
mRNA expression (fold change)
J
Plasma IL-6 ELISA
IL-6 (pg/mL)
K
Delta change Body Mass
Days Post Implantation
Body mass change (% initial)
Sham
OT-KxPxCx^{IL6} IgG Control
OT-KxPxCx^{IL6} CD4/8 Depleted
L
Gastrocnemius Mass
mass (mg/g baseline BM)
M
Gastrocnemius Gene Expression
mRNA expression (fold change)
Trim63
Fbxo32

Figure 6

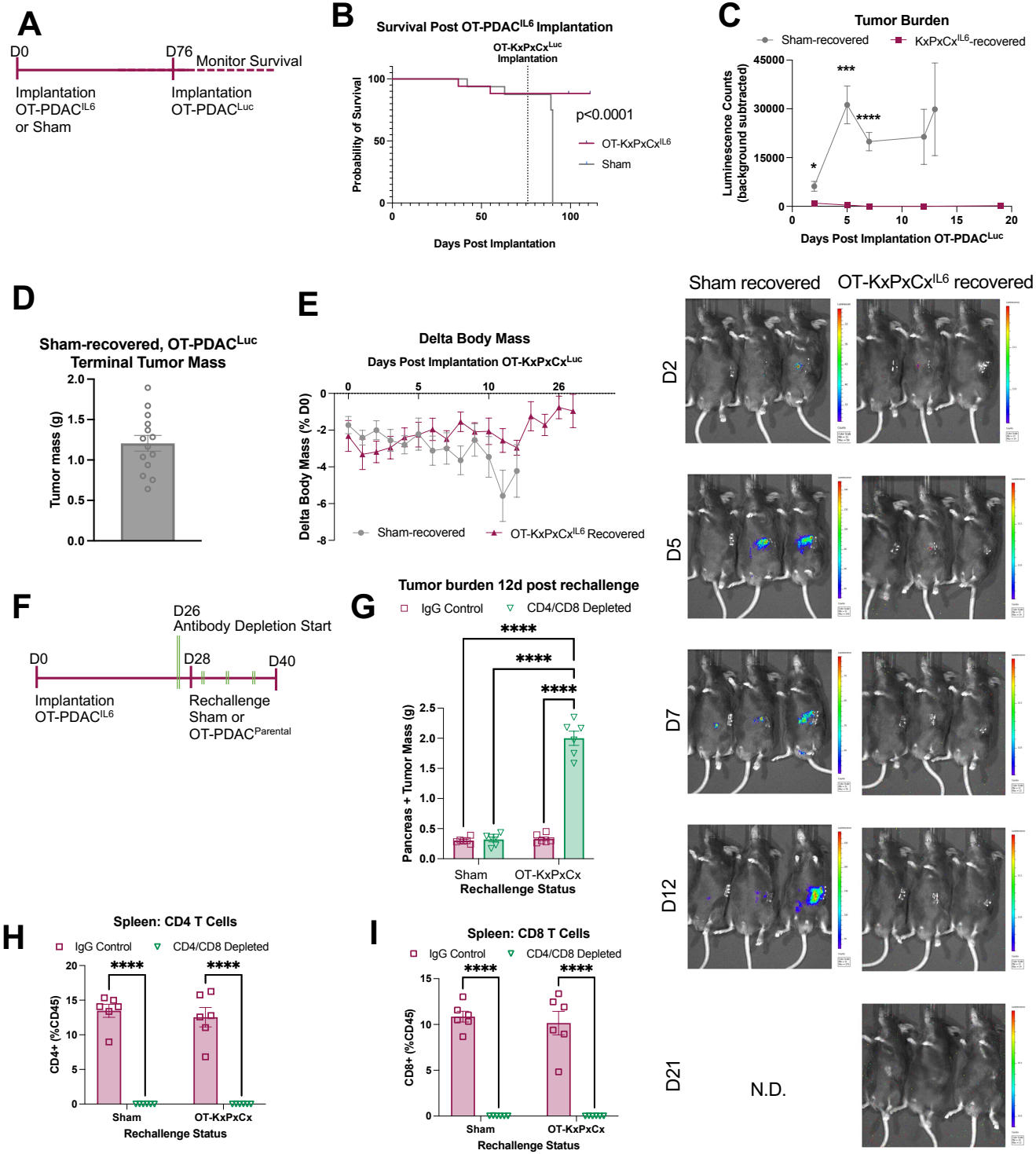
A
D0
D76
Monitor Survival
Implantation OT-PDAC^{IL6} or Sham
Implantation OT-PDAC^{Luc}
B
Survival Post OT-PDAC^{IL6} Implantation
OT-KxPxCx^{Luc} Implantation
Probability of Survival
p<0.0001
OT-KxPxCx^{IL6}
Sham
Days Post Implantation
C
Tumor Burden
Sham-recovered
KxPxCx^{IL6}-recovered
Luminescence Counts (background subtracted)
Days Post Implantation OT-PDAC^{Luc}
D
Sham-recovered, OT-PDAC^{Luc} Terminal Tumor Mass
Tumor mass (g)
E
Delta Body Mass
Days Post Implantation OT-KxPxCx^{Luc}
Delta Body Mass (% D0)
Sham-recovered
OT-KxPxCx^{IL6} Recovered
Sham recovered
OT-KxPxCx^{IL6} recovered
D2
D5
D7
D12
D21
N.D.
F
D26
Antibody Depletion Start
D0
D28
D40
Implantation OT-PDAC^{IL6}
Rechallenge Sham or OT-PDAC^{Parental}
G
Tumor burden 12d post rechallenge
IgG Control
CD4/CD8 Depleted
Pancreas + Tumor Mass (g)
Sham
OT-KxPxCx
Rechallenge Status
H
Spleen: CD4 T Cells
IgG Control
CD4/CD8 Depleted
CD4+ (%CD45)
Sham
OT-KxPxCx
Rechallenge Status
I
Spleen: CD8 T Cells
IgG Control
CD4/CD8 Depleted
CD8+ (%CD45)
Sham
OT-KxPxCx
Rechallenge Status

Figure 7

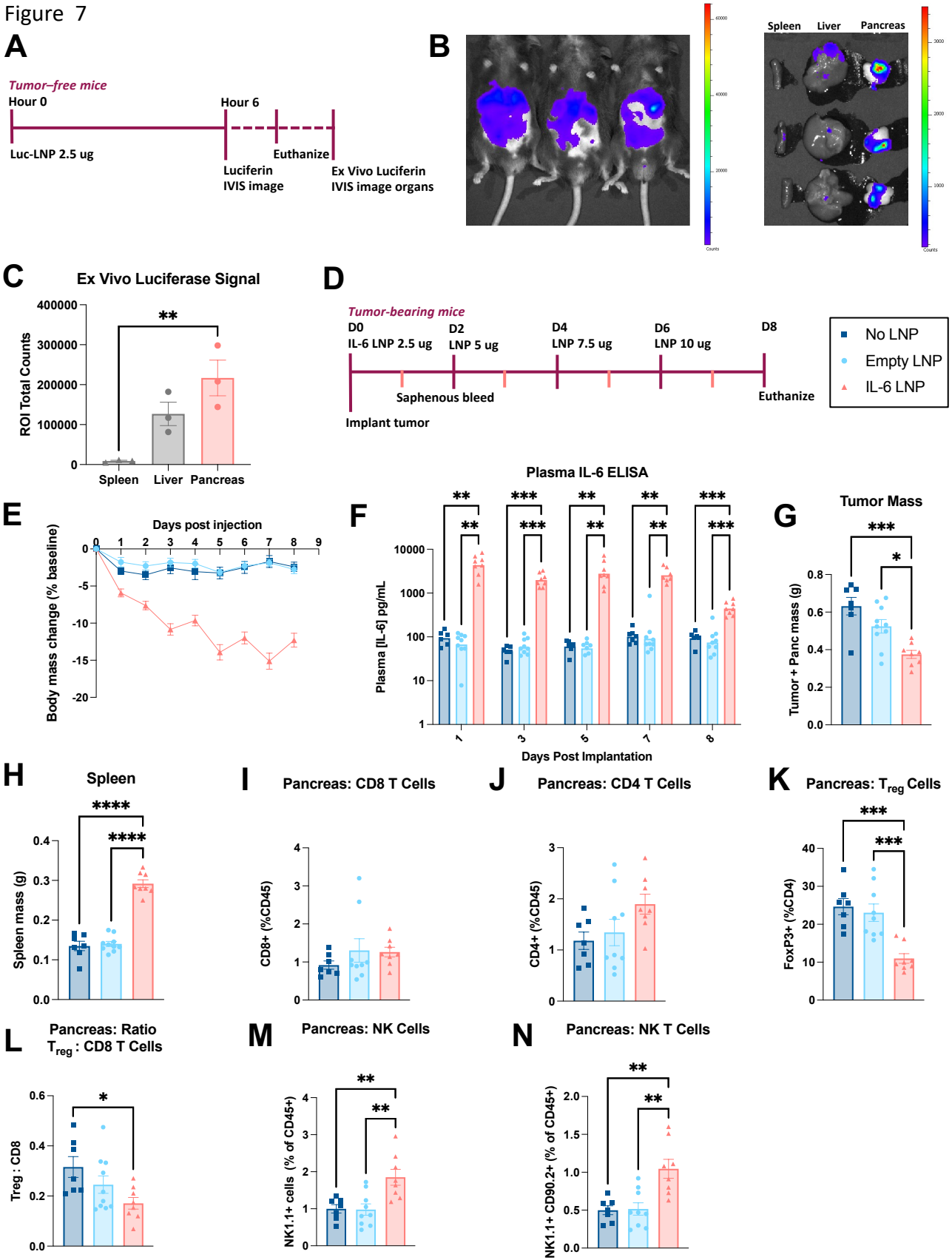
A
Tumor–free mice
Hour 0
Hour 6
Luc-LNP 2.5 ug
Luciferin
IVIS image
Euthanize
Ex Vivo Luciferin
IVIS image organs
B
Spleen
Liver
Pancreas
C
Ex Vivo Luciferase Signal
ROI Total Counts
400000
300000
200000
100000
0
**
Spleen
Liver
Pancreas
D
Tumor-bearing mice
D0
IL-6 LNP 2.5 ug
D2
LNP 5 ug
D4
LNP 7.5 ug
D6
LNP 10 ug
D8
Saphenous bleed
Implant tumor
Euthanize
No LNP
Empty LNP
IL-6 LNP
E
Days post injection
Body mass change (% baseline)
0
-5
-10
-15
-20
F
Plasma IL-6 ELISA
Plasma [IL-6] pg/mL
10000
1000
100
10
1
Days Post Implantation
G
Tumor Mass
Tumor + Panc mass (g)
0.8
0.6
0.4
0.2
0.0
***
*
H
Spleen
Spleen mass (g)
0.4
0.3
0.2
0.1
0.0
****
I
Pancreas: CD8 T Cells
CD8+ (%CD45)
J
Pancreas: CD4 T Cells
CD4+ (%CD45)
K
Pancreas: Treg Cells
FoxP3+ (%CD4)
40
30
20
10
0
L
Pancreas: Ratio
Treg : CD8 T Cells
Treg : CD8
0.6
0.4
0.2
0.0
M
Pancreas: NK Cells
NK1.1+ cells (% of CD45+)
N
Pancreas: NK T Cells
NK1.1+ CD90.2+ (% of CD45+)
2.0
1.5
1.0
0.5
0.0